Estimating surface water availability in high mountain rock slopes using a numerical energy balance model

Matan Ben-Asher[1], Florence Magnin[1], Sebastian Westermann[2], Josué Bock[1], Emmanuel Malet[1], Johan Berthet[3]~~, Josué Bock[1]~~, Ludovic Ravanel[1], Philip Deline[1].

[1]EDYTEM laboratory, Université Savoie Mont Blanc, CNRS, Le Bourget-du-Lac, 73376, France.
[2]Department of Geosciences, University of Oslo, Oslo, Norway.
[3]Styx 4D, Le Bourget du Lac, France.

Correspondence to: Matan Ben-Asher (matan.ben-asher@univ-smb.fr)

Abstract

Water takes part in most physical processes that shape the mountainous periglacial landscapes and initiation of mass wasting processes. An observed increase in rockfall activity in ~~several mountainous~~high mountains regions was previously linked to permafrost degradation~~ in high mountains~~, and water that infiltrates into rock fractures is one of the likely drivers of ~~these~~ processes related to thawing and destabilization. However, there is very little knowledge ~~on~~of the quantity and timing of water availability for infiltration in steep rock slopes. This knowledge gap originates from the complex meteorological, hydrological, and thermal processes that control snowmelt, and also the challenging access and data acquisition in ~~the~~ extreme alpine environments. Here we use field measurement and numerical modeling to simulate the energy balance and hydrological fluxes in a steep high elevation permafrost-affected rock slope at Aiguille du Midi (3842 m a.s.l, France), in the Mont-Blanc massif. Our results provide new information about water balance at the surface of steep rock slopes. Model results suggest that only ~25% of the snowfall accumulates in our study site, the remaining ~75% ~~are redistributed~~is likely transported downslope by wind and gravity. ~~Snow accumulation depth~~The snowpack thickness is inversely correlated with surface slopes between 40° to 70°. We found that among all water fluxes, sublimation is the main process of snowpack mass loss in our study site and generally in the high-altitude environment. Snowmelt occurs between spring and late summer ~~and~~but most of it ~~does~~may not reach the rock surface due to refreezing and the formation of an impermeable ice layer at the base of the snowpack~~.~~, which was observed in the field site. The annual ~~effective~~ snowmelt~~,~~ that is available for infiltration~~,~~ (i.e. effective snowmelt) is highly variable ~~and ranges over a factor of six with values between 0.05-0.28 m in the~~in the simulated years 1959-2021~~. The~~ and its onset ~~of the effective snowmelt~~ occurs mostly between May and August~~,~~ and ends before October. ~~It precedes the first rainfall by one month on average. Sublimation is the main process of snowpack mass loss in our study site. Model simulations at varying elevations~~By applying the model to a range of altitudes, we show that effective snowmelt is the main source of water for infiltration above 3600 m a.s.l.; below, direct rainfall on snow-free surface is the dominant source. ~~The~~This change from snowmelt-~~dominated~~ to rainfall-dominated water ~~availability is nonlinear and characterized by a rapid~~input leads to an abrupt, non-linear increase in water availability ~~for infiltration. We suggest that this elevation~~at altitudes below 3600 m a.s.l

and may point to higher sensitivity of ~~water availability transition is highly sensitive to climate change, if snowmelt-dominated~~ permafrost-affected rock slopes ~~experience an abrupt increase in water input that can initiate rock slope failure~~to climate change at these altitudes.

1 Introduction

~~1.1. Water in high mountain periglacial rock slopes~~

Water plays a key role in the ~~initiation of mass wasting~~thermal and mechanical processes in mountainous periglacial landscapes and can influence the stability of steep rock slopes in several ways (French, 2017)~~.~~. Surface water that infiltrates into rock fractures can efficiently transport heat by advection and lead to ~~deep permafrost degradation with~~ a thicker and earlier development of the active layer (i.e. the depth of seasonal thawing) in permafrost-affected ground, as compared to pure heat conduction (Hasler et al., 2011; Magnin and Josnin, 2021; Gruber and Haeberli, 2007). The warming of permafrost-affected rock slopes can potentially decrease the rock's uniaxial and tensile strength (Krautblatter et al., 2013; Dwivedi et al., 1998; Li et al., 2003; Mellor, 1973)~~Water infiltration is also responsible for mechanical weakening of the rock~~ and also reduce friction along joints and ice-bonded discontinuities (Haeberli et al., 2010; Mamot et al., 2018, 2020). In ~~large~~addition, the accumulation of water in deep fractures~~, moving water can create thawing corridors extending deep into permafrost . Percolation of water into the tunnels of the Aiguille du Midi (French Alps) cable-car station, noticed every hot summer since the summer heatwave of 2003, is likely caused by this effect (Gruber and Haeberli, 2007). Accumulation of water in deep fractures can potentially result in a~~ can lead to a high enough hydrostatic head ~~high enough~~ to exert ~~sufficient~~critical pressure ~~to initiate~~and initiation of failure (Fischer et al., 2010). Water ~~is~~that refreezes in saturated fractures can also build up critical cryostatic pressure (Matsuoka, 2008; Draebing and Krautblatter, 2019)~~an important driver of near surface weathering processes such as frost cracking and acceleration of subcritical cracking~~. Over geological time scales water is an important catalyst of mechanical rock weathering processes related to subcritical cracking (Eppes and Keanini, 2017). However, despite the existing knowledge and ongoing research on water-related mechanical processes in mountainous periglacial landscapes, little knowledge exists on the quantity and timing of water ~~available for infiltration~~availability in these environments. This knowledge is becoming ~~increasingly needed~~even more imperative with the fast warming of high permafrost-affected mountain regions (Haeberli and Gruber, 2009)~~, permafrost warming~~ , and the growing evidence for a related increase in rockfall occurrence (Gruber et al., 2004; Allen et al., 2009; Ravanel and Deline, 2011; Huggel et al., 2012; Ravanel and Deline, 2013; Ravanel et al., 2017)~~as thawing corridors can contribute to the destabilization of large rock volumes, much more than expected in a purely conductive system .~~.

This study is aimed to decipher the availability of surface ~~moisture availability in steep mountain landscapes and to evaluate its role in~~water for surface ~~processes and permafrost degradation~~and hydrological processes. To do so, we use a numerical energy balance model coupled with a state-of-the-art snowpack scheme, forced by field measurements and reanalysis of meteorological datasets, to simulate ~~the~~ hydrological and thermal processes ~~mentioned above~~at the surface, and quantify the flux of excess water that is available for infiltration.

~~1.2. Estimating snow accumulation and snowmelt on steep slopes~~

~~Precipitation in high mountains~~Snowmelt is ~~composed mostly of snowfall . We thus expect snow to be the main~~a major source of water in high mountains, however, despite its fundamental importance, we lack a robust understanding of its rates and timing. A significant portion of the snow that falls on steep slopes does not accumulate due to redistribution by wind and transport by gravity (Sokratov and Sato, 2001; Mott et al., 2010), and snowfall measurement techniques commonly introduce large errors, especially in windy conditions (Rasmussen et al., 2012)~~.~~. We thus differentiate between rates of snow accumulation and snowfall. Previous studies suggested that snow accumulation on steep rock slopes is inversely proportional to the slope angle and that above a certain slope angle, snow does not accumulate (Blöschl et al., 1991; Winstral et al., 2002; Gruber Schmid and Sardemann, 2003; Haberkorn et al., 2015; Sommer et al., 2015). Existing estimations of the threshold angle for snow accumulation range between 45°-80°. This wide range is likely due to differences in local climatic and topographic conditions in different study areas (Phillips et al., 2017), and perhaps also the resolution of the topographic data used in the analysis (Blöschl et al., 1991; Haberkorn et al., 2017). In this study, we use a site-specific analysis of snow depth distribution from a repeated high-resolution survey of our study site using drone-based photogrammetry. This information is essential to ~~estimate~~accurately model the snow water equivalent amount at the rock slope surface. However, ~~estimations of the~~quantifying water equivalent snowmelt ~~are~~is not enough to evaluate infiltration potential since the actual flux that is available for infiltration is also controlled by the hydrological properties of the snowpack and the rock itself. Snowmelt that percolates to the base of the snowpack can refreeze to form an impermeable basal ice layer at the interface between the snow cover and the rock surface~~,~~ when the rock surface is cold enough to dissipate the latent heat of freezing (Woo and Heron, 1981; Woo et al., 1982; Marsh, 2005; Fierz et al., 2009) (Supp fig. S1). This ice crust phenomenon was described by Phillips et al. (2016) in an alpine permafrost-affected rock ridge, where they used borehole temperature ~~(T)~~ data to demonstrate how a basal ice layer ~~prevents~~, which they observed in monitored snow pits, limits the infiltration of spring snowmelt. To differentiate from the ~~total~~net snowmelt, we use the term 'effective snowmelt' referring to excess water that ~~exceed~~exceeds the field capacity of the snow and ~~occur~~occurs when the base of the snowpack is permeable and enables infiltration to the rock surface (*i.e.*, when no ice crust exists).

2 Study area

The Mont Blanc massif covers approximately 550 km² across France, Italy, and Switzerland (Fig. 1). It is predominantly composed of crystalline rocks with a Hercynian granitic batholith dated at 304 ± 3 Ma intruded in a metamorphic (mostly gneisses and mafic schists) basement dated at 453 ± 3 Ma (Bussy and Von Raumer, 1994; Leloup et al., 2005). Shear zones and faults networks, mainly striking 0° N to 25°E and 45°N to 60°E (Rossi et al., 2005), outline the main peaks, spurs, and couloirs with their sub-vertical dipping characterized by a fan-like arrangement across the range, being slightly inclined towards south-east (SE) in the north-west (NW) part of the massif and towards NW in its SE part (Bertini et al., 1985).

The massif is one of the most glaciated over the western European Alps with about 102 km^2 of glaciers in 2007-2008 (Gardent et al., 2014) extending from the Mont Blanc summit at 4808 m a.s.l. down to the toe of the Bossons glaciers at c. 1450 m a.s.l. Its steep rock walls that frequently reach altitudes above 4000 m a.s.l are also strongly affected by permafrost whose lower elevation is found around 2600 m a.s.l in north faces to 3200 m a.s.l in south faces (Magnin et al., 2015a). These lower limits may vary by several hundreds of meters, depending on the surface conditions such as fracture density and snow cover (Boeckli et al., 2012). Since the 1990s, these rock walls have been affected by an increasing amount of rockfalls (Ravanel and Deline, 2011), with particularly high frequencies during hot summers, such as 2003 and 2015, occurring across a wide range of elevations from 2700 to 4000 m a.s.l. (Ravanel et al., 2017).

The Aiguille du Midi (~~AdM) (~~3842 m a.s.l.; 45.88~~°~~° N, 6.89~~°~~° E) is located on the north-west side of the Mont-Blanc massif (Fig. ~~1).~~1) in the porphyritic granite zone. Its summit consists of three steep peaks (North, Central, and South). The ~~north and west faces~~peaks tower more than 1000 m above the Glacier des Pélerins and Glacier des Bossons, ~~while~~on the north and east faces, and the south face is ~~only~~ 250 m high above the Glacier du Géant~~. The bedrock is composed of porphyritic granite characterized by a N 40° E fault network intersected by a secondary network .~~. The combination of various slope angles and surface characteristics at the Aiguille du Midi makes it particularly representative of the Mont Blanc massif rock walls. A tourist cable car runs from Chamonix to the ~~AdM~~Aiguille du Midi North peak, where galleries and an elevator are carved in the rock mass~~ and provide~~, providing year-round access to an extreme and otherwise inaccessible environment. Furthermore, alongside the steep vertical rock walls, slopes with intermediate angles (50-60°) and rugged surfaces allow the accumulation of a thick snow cover (> 0.6-0.8 m) throughout the winter, resulting in variable permafrost conditions from warm discontinuous permafrost on the SE face to vertical rock slabs affected by cold and continuous permafrost on the NW (Magnin et al., 2015b). This makes the Aiguille du Midi an ideal location to study processes of high, permafrost affected, mountain landscapes. The study site used for the main analysis is ~~located~~ in a ~500 m^2 rock slope on the central pillar's SE face (azimuth angle 150°) ~~face of the central pillar~~ with an average slope ~~of 55°. The~~angle of 55° (Fig. 1). It is located below a confined section of the touristic structure and it is not frequented by skiers and alpinists. There is thus minimal man-made influence on the natural processes of snow accumulation. The SE study site ~~is~~was surveyed and equipped with ~~a borehole for T measurements to a depth of 10 m since December 2009 fitted with 10 m length Stump thermistor chains, each with 15 nodes (YSI 44031 sensors, accuracy ±0.1°C). There are also repetitive high-resolution 3D photogrammetric survey,~~several monitoring systems that support the research presented in this contribution, and detailed in the methods section, including a time-lapse camera and snow depth measurement poles to monitor temporal changes in snow accumulation (see Fig. 1, Fig. 4 and section 3.2), 10 m deep boreholes with temperatures sensors (Fig.1B), and repeated high resolution 3D topographic surveys of the surface with minimal snow cover, and after substantial snowfall (see Fig. 2 and section 3.1). A second site on the E side of the central pillar was used to validate the results and includes a 10 m deep borehole, time-lapse camera records, and snow depth measurement poles.

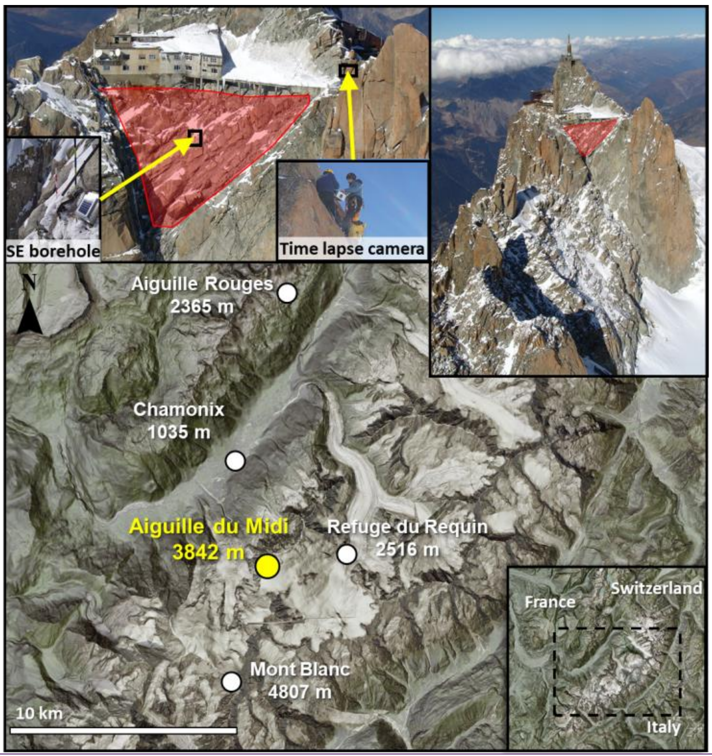
SE borehole
Time lapse camera
N
Aiguille Rouges
2365 m
Chamonix
1035 m
Aiguille du Midi
3842 m
Refuge du Requin
2516 m
Mont Blanc
4807 m
10 km
France
Switzerland
Italy

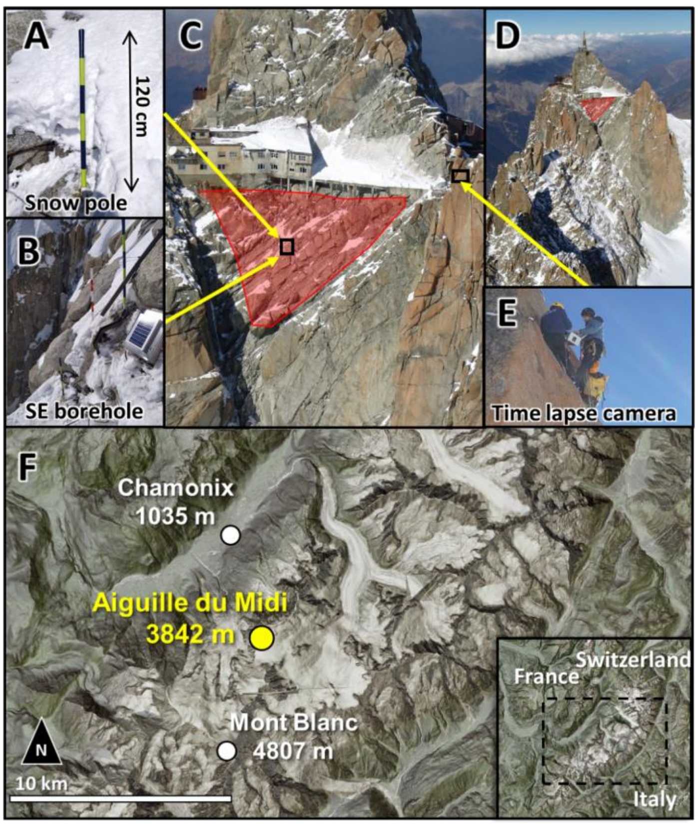

Figure 1: Location map of the study ~~sites and inset map~~site. A) Snow accumulation measurement pole. B) Southeast location of the ~~Mont-Blanc massif. Top images show the~~borehole with logger box and solar panel. C-D) Study site on the SE face of Aiguille du Midi ~~(AdM).~~. Red polygon shows the slope area surveyed for high-resolution topography using a drone. ~~The small image shows the snow accumulation poles and the borehole on the left, and a time~~ E) The time-lapse camera installed on the SE pillar ~~on the right, with yellow arrows pointing to their location on the rock slope~~. F) General location in the Mont Blanc massif. Maps provided by the Federal Office of Topography swisstopo.

3 Methods

3.1. Snow depth – spatial distribution

Snow accumulation is simulated in our model setup and field measurements are used in the validation process. To analyze the spatial distribution of snow depth in our study site, we produced two 3D photogrammetric point cloud models of an area of ~500 m^2 on the SE slope rock surface: one with minimal snow cover, ~~in~~on October 27th 2021, and another with substantial snow cover following ~~heavy snowfall in~~on January 17th 2022 (Fig. 2A-B). Based on our knowledge of the site (first fieldwork in 2005), we assume that the January 2022 snow cover represents conditions close to maximal accumulation. Data from an on-site time-lapse camera (see section 3.2) and from a meteorological station in Chamonix show that substantial snowfall events occurred on the 25th to 27th of December and 5th to 7th of January. We assume that the 10 days without snowfall before the survey was sufficient for preliminary redistribution and compaction processes to take effect and that further processes of mass loss from the snowpack are either by sublimation or snowmelt.

The use of high-resolution photogrammetric 3D models from drones has become a prevalent method in geomorphology, particularly in high mountain regions (e.g. Tonkin et al., 2016; Vivero and Lambiel, 2019). However, obtaining data on high mountain walls using drones can be a demanding and complex task. The challenging topography necessitates increased flight precautions. In the current study, flight was performed in a manual mode at approximately 30 meters from the wall, to achieve a satisfactory overlap rate and a view angle perpendicular to the slope. Table 1 presents a summary of the characteristics of the two flights and the point clouds in the region of interest.

Field conditions on the South face of the Aiguille du Midi did not allow the use of ground control points (GCPs). The use of GPS in these environments does not provide satisfactory precision due to the satellite masking effect created by the walls. It was also not possible to perform topographic measurements, and the Real-Time-Kinematic (RTK) positioning system of the drone was not functional during manual flight. Furthermore, there was no access to high-resolution 3D models (terrestrial or airborne LiDAR) which would have allowed for georeferencing through coregistration from pre-georeferenced point clouds. Since absolute georeferencing was not necessary, we chose to work solely using the georeferencing and exterior orientation parameters of the images measured by the GPS/IMU systems onboard the drones (Essel et al., 2022). This method allows for the creation of a 3D model with satisfactory relative accuracy, with global geometric errors below 0.5%, and even offers better performance in the Z-axis than using RTK-based georeferencing (Jain, 2021). These parameters are managed in the version of Metashape used to create the 3D models. Subsequently, we performed the coregistration of the second drone survey on the first, using 19 GCPs identified as common distinctive points between the two models in the region of interest.

Table 1: Characteristics of UAV flights, point clouds, and comparison uncertainties

Date of flight	27/10/2021	17/01/2022
Drone	DJI Phantom 4 RTK	Parrot Anafi AI

Camera sensor	CMOS 1" 20M Pixel	CMOS 1/2" 48M Pixel
Flight mode	Manual	Manual
Number of photographs	269	326
Number of points on the ROI	1532309 pts	1214577 pts
Mean point density on the ROI	1799 pts/m²	1379 pts/m²
M3C2 Lod	0.071m	
M3C2 RMSE	0.13m	

The uncertainty of the comparison (Table 1) was obtained through the statistical analysis of point-to-point distances between the two-point clouds, calculated using the M3C2 module of CloudCompare, on surfaces identified as stable between the two models, where the expectation of measurement is zero. The distances measured on these surfaces are therefore measurement errors. The Root Mean Square Error (RMSE) is calculated as the component of systematic errors (Mean) and standard deviation (σ) by the following formula:

$$RMSE = \sqrt{\sigma^2 + Mean^2} \quad (1)$$

The Level of Detection (LoD) is defined as the 95% confidence interval of the vertical error, the standard deviation of the RMSE (Zhang et al., 2019) :

$$LoD = 1.96RMSE \quad (2)$$

The point clouds were compared by interpolating the elevation data into a 0.1 m cell-size digital elevation model (DEM). We calculated the local slope and vertical snow depth for each grid pixel (Fig. 2 C-D). The angle of the rock slope surface was calculated by fitting a second order polynomial surface to a window size of 3×3 pixels and deriving the local gradient (Zevenbergen and Thorne, 1987; Evans, 1980)~~.~~ from the DEM of the snowless conditions (Zevenbergen and Thorne, 1987; Evans, 1980). The main purpose of this analysis was to examine the relation between snow depth and local slope, and also to compare with data from our time-lapse camera (see 3.2) to determine the maximum snow depth. We compared the 0.1 m slope-depth relation (Fig. 2C-D) with an upscaled 1 m resolution grid (Fig. 2E-F), which is the length scale of our model realizations, and found the results to be in good agreement~~.~~, as shown by the comparison between slope angle distributions of the two resolutions (Fig.2D and 2F).

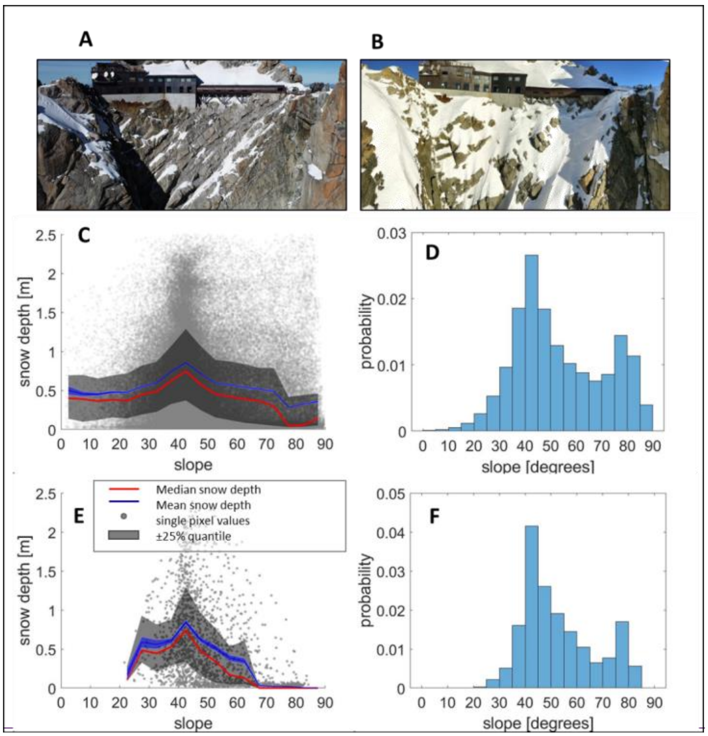
A
B
C
D
E
F
snow depth [m]
slope
probability
slope [degrees]
Median snow depth
Mean snow depth
single pixel values
±25% quantile

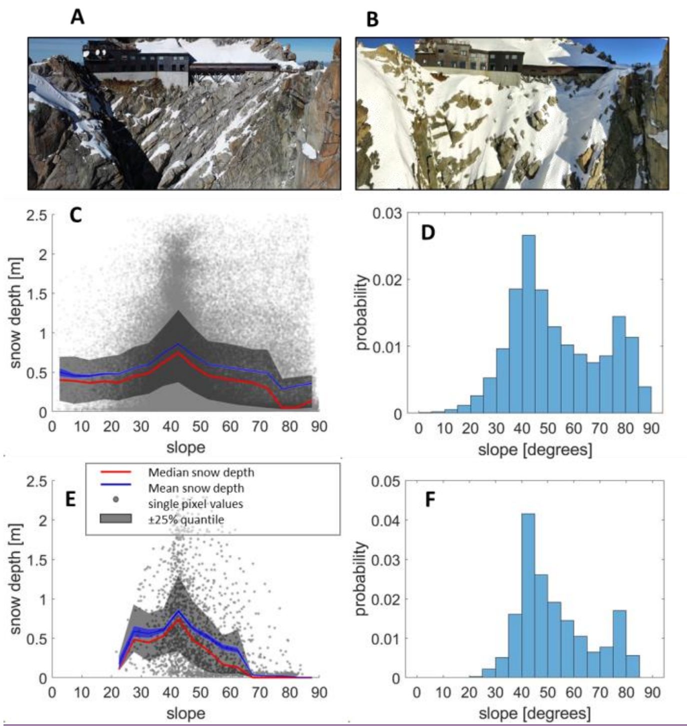

Figure 2: Snow accumulation on ~~steep~~ rock walls - Snow depth vs. local slope from the comparison of two 3D photogrammetric point cloud models of an area of 500 m^2 on the SE slope rock surface. A) SE face of ~~AdM~~Aiguille du Midi with minimal snow cover in October 2021. B) SE face of ~~AdM~~Aiguille du Midi with substantial snow cover in January 2022. C) Snow depth as a function of the local slope of the 0.1 m pixels in a high-resolution DEM. Red line is the median value of snow depth for bins of specific local slope (bin size=5º) with ±25% quantile range in gray. Blue line is the mean value with a range of ± standard error. D) Distribution of local slope values. Vertical axis is probability. (E-F) Same as C-D after resampling the point cloud data to 1 m cell size. Note that snow depth systematically decreases from a median depth of ~~70 cm at~~0.7 m (average depth 0.8 m) for a slope of 40° ~~(and average depth of 80 cm)~~ to <~~10 cm~~0.1 m at 70° slope.

3.2. Snow depth – temporal distribution

~~We used time~~ Time-lapse cameras with a temporal resolution of ~~several~~4 images per day were used to monitor the height of accumulated snow using permanent measurement poles installed ~~in~~on our study site ~~in AdM~~at Aiguille du Midi (Fig. 1, 4B). ~~We installed 5~~The snow depth data covers periods between 2012-2015 and 2021-2022. Ten poles ~~in an area~~were installed in two areas of 20 m × 20 m each, near the ~~borehole~~boreholes on the SE face~~. We used also data that was collected in the same~~

~~method in 2012 on the~~ (Fig. 1) and on the east (E) face~~, near the E borehole. Each pole is 1.4~~. The poles heights are 1-1.35 m ~~high~~ and painted with colored ~~scales~~bands of 0.1/0.2 m. ~~We produced a~~ Snow accumulation time series, with a sub-daily resolution, were then produced by visually examining the images with an estimated accuracy of ~ ~~5 cm.~~0.1 m, based on the ability to read the snow depth ~~time series~~ from ~~our~~the images. A snow depth time series of the SE face field site ~~were then~~, based on images taken between January 2012 and July 2012, from the same camera position, was used to calibrate the model ~~constrains~~constraints on snow accumulation and loss rates, and ~~determine~~also compare with the maximum snow depth~~. In addition, we used available snow depth measurement from *in-situ* meteorological stations in the Mont-Blanc massif and its area at the Refuge du Requin (https://www.fondation-eng.org/station-meteo) (2516 m a.s.l.) and Aiguilles Rouges – Nivose (*Météo-France*~~ values obtained from the 3D photogrammetric point cloud models. A snow depth time series of the E face, from images taken between February 2012 and January 2015 (with gaps in data~~) (2365 m a.s.l.) (Fig. 1) to compare with the temporal variations in our model results. We assume that the timing of snowfall and accumulation shows a similar trend at the AdM, although the topography and elevation are different~~ between June 2012 and ~~likely to affect the maximum depth. For this reason, we normalized the snow depth at Refuge du Requin and Aiguilles Rouges to the maximum snow depth used in the model run: 80 cm.~~

~~1.3. Borehole rock temperature profile~~

~~Three boreholes were drilled in 2009 and equipped with T sensors to a depth of ~10 m in 2010 . T sensors depths in the SE borehole are: 0.3, 0.5, 0.7, 0.9, 1.1, 1.4, 1.7, 2.0, 2.5, 3.0, 4.0, 5.0, 7.0, 9.0, 10.0 [m], and in E borehole are: 0.14, 0.34, 0.74, 1.04, 1.34, 1.64, 2.14, 2.64, 3.64, 4.64, 6.64, 8.64, 9.64 [m]. The average T in each depth is stored at time steps of 3 hours. The time *vs* depth measurements of rock T were~~March 2013) was used to validate the ~~numerical energy balance~~ model.

3.3. ~~Modeling~~Simulating snow evolution with a surface energy balance model

~~1.3.1. Model setup~~

3.3.1. The CryoGrid community model

The CryoGrid community model is a toolbox for numerical simulations of ground thermal regime and water balance. Its modular structure makes it suitable for a wide range of terrestrial cryosphere settings and is mainly applied in permafrost environments (Westermann et al., 2022)~~.~~, using the finite-difference method to transiently simulate ground temperatures and water balance. Previous studies successfully used former CryoGrid models to simulate processes in steep rock walls and mountainous regions (Magnin et al., 2017; Myhra et al., 2017; Schmidt et al., 2021; Legay et al., 2021). We used the CryoGrid community model (version 1.0) toolbox (Westermann et al., 2022) to simulate the one-dimensional (1D) ground thermal regime and ice/water balance~~,~~ and estimate the availability of surface water and its potential for infiltration in rock fractures. The ground domain, representing the rock wall, is simulated as a 1D gridded column with a depth of 100 m. Ground temperatures are calculated using diffusion and advection by vertical water flow. The lower boundary condition is provided by a constant geothermal heat flux. The upper boundary is calculated by surface energy balance using atmospheric forcing (see section 3.3.2). Water balance and hydrological processes are also simulated. We used a water scheme based on Richard's equation (Richards, 1931) of unsaturated flow to simulate flow in the rock. We applied a low porosity value (1%) to limit infiltration and conserve the full potential of excess water at the surface in each time step (i.e. the amount of water that could potentially infiltrate if a fracture exists). In addition to surface energy balance, the CryoGrid model is implemented with the state-of-the-art CROCUS snow scheme (Vionnet et al., 2012) which provides representations of snow cover dynamics, and water drainage. The CROCUS scheme allows for transient representation of internal snow properties as well as processes of interaction between atmosphere, snow, and rock (supp. Fig. S2). Snow surface mass fluxes are also computed with the consideration of energy balance and include latent heat fluxes from evaporation and sublimation following an approach by Boone and Etchevers (2001)~~interaction processes with the atmosphere and rock (supp. Fig. S2). To model water balance at the rock surface,~~. Water flow in the snowpack is simulated with a scheme that includes a threshold value of field capacity. At values below the threshold no flow occurs, and above it, flow is governed by gravity and the hydraulic conductivity of the snow. We consider two potential sources of water for infiltration into rock fractures: rainfall and snowmelt. Excess water was set to be produced during snowmelt and rainfall in scenarios when snow water content exceeds its saturated field capacity, if snow cover exists.~~ Snow hydrology is simulated as vertical flow driven by gravity.~~

~~3.3.1.~~3.3.2. Forcing Data

Obtaining reliable and continuous long-term meteorological data from high mountain regions is challenging due to the extreme conditions that limit accessibility and damage equipment. Thanks to the accessibility of the ~~AdM~~Aiguille du Midi site, meteorological data is available from *in-situ* meteorological stations, including a permanent station of *Météo France* running since 2007. However, the available meteorological data sets contain large gaps and are of limited ~~most~~ duration. We thus compared the available measurements of air temperature at Aiguille du Midi and precipitation at the nearby station of Chamonix with data obtained from the S2M-SAFRAN meteorological reanalysis tool~~ and~~. We found it well fitted for our needs, with R^2 values of 0.97 and 0.69 for air temperatures and precipitation, respectively (supp. Fig. S3). The S2M-SAFRAN dataset combines output from a numerical weather prediction model and *in situ* observations~~,~~ and was originally developed for operational needs to estimate avalanche ~~hazard~~hazards in mountainous areas (Durand et al., 1993). ~~The S2M-SAFRAN dataset~~ It is available for ~~various~~74 mountain areas~~,~~ in France, including the Mont Blanc massif, with an area of 585 km^2 and 26 meteorological stations used in the reanalysis of this area. The data in each area is divided at elevation steps of 300 m, ~~and~~ with an hourly resolution between the years 1958 to 2021 (Vernay et al., 2022). ~~It~~The S2M-SAFRAN data set includes most parameters that are required for modeling with CryoGrid: relative humidity, air ~~T~~temperature, incoming long ~~wavelength~~

~~radiation, incoming~~ and short wavelength ~~solar~~ radiation, and wind speed. To complete the forcing data, we used top of the atmosphere incident solar radiation from ERA5 global reanalysis dataset (Hersbach et al., 2020).

~~1.3.2. Calibration~~Constraining snow accumulation and ~~validation~~

3.3.3. ~~Our approach to calibrate the~~ model ~~was to fix most~~ calibration

Our model setup contains uncertainties regarding unknown model parameters ~~with known physical parameters of the study site from~~which we estimated using the literature (Table ~~1)~~ 2) (Legay et al., 2021; Magnin et al., 2017) and ~~calibrate the model using two parameters that have predominant impact~~calibration. Two of the model outputs can be compared with field measurements and were used for calibration – snow depth, which has a direct influence on ~~snow accumulation:~~ water availability, and near surface temperature which can indirectly influence the water mass balance by controlling sublimation, evaporation, melting, and refreezing of the snow. We used a parameter named "snowfall multiplication factor~~, and maximum snow depth. The snowfall multiplication factor is~~", which has a constant value between 0-1 that sets the fraction of snowfall, provided by the meteorological dataset, that ~~can accumulate~~ accumulates on the surface. For example, a snowfall ~~fraction~~ multiplication factor value of 0.25 means that only 25% of the net ~~snow fall~~snowfall is accumulated. ~~Maximum~~Another constraint on snow ~~depth~~accumulation used in the model is the value of maximum snow depth. It is the ~~maximal~~maximum depth above which no snow can accumulate once it is reached. The value of maximum snow depth was obtained by comparing two 3D high-resolution models of the study site in snow-free conditions and after heavy snowfall and was found to be slope dependent (see ~~sect.~~sections 3.1~~). For~~ and 4.2). In the calibration~~, we used two model outputs that impact snowmelt and that process,~~ we ~~have field data to compare them with~~aimed to optimize two model outputs: snow depth and near surface ~~T. We made model runs while iterating over a range of snowfall fraction values and maximum snow depth, and looked for the optimized R² and RMSE values of the correlation between observed and modeled near surface T~~temperature, by comparing them with field measurements (Fig. 3B). ~~Following the calibration procedure, we~~The model was validated ~~the model by modeling the T at~~by simulating the E face of ~~AdM~~Aiguille du Midi using the calibrated model parameters ~~from these faces.~~(calibrated with data from the SE face). The location of the validation site on the E face ~~borehole~~ shares many characteristics with the SE face borehole (*i.e.* elevation, ~~slope,~~ rock type, ~~meteorology).~~climate) and includes the required datasets that were used in the calibration – snow depth poles, a time-lapse camera and near surface temperature measurement in a 10 m deep borehole. However, for technical reasons, the borehole on the E face was originally installed in a sub-vertical wall that does not accumulate snow. We thus compared the near-surface ~~T~~temperature measured at the E face with the modeled ~~one~~temperature with a low snowfall multiplication factor value of 0.1 (10%) (Fig. 3C~~). A north facing borehole also exist at AdM but its location in a vertical wall, above a ledge that locally accumulates snow, makes it impractical for our model settings.~~), and measured snow accumulation with the calibrated value of 0.25 (25%) (supp. Fig. S4).

~~**Table 1: Model parameters**~~

Parameter	Value	Units	Source	~~**Remarks**~~
volumetric heat capacity mineral	2×10^{6}	J/m^3K	1	
thermal conductivity	3.3×10^{-3}	W/K	1	
sky view factor	0.63		Calculated using QGIS	
~~snow fraction~~snowfall multiplication factor	0.25		Calibrated	
heat flux at lower boundary	-0.25	W/m^2	2	
surface albedo	0.16		2	
surface emissivity	0.92		3	
roughness length	0.01	m	2	
maximum snow depth	0.8	m	Field measurement	~~For slope angle 45°~~

[1]Legay et al. (2021)
[2]Magnin et al. (2017)
[3]Mineo and Pappalardo (2021)

Deleted Cells

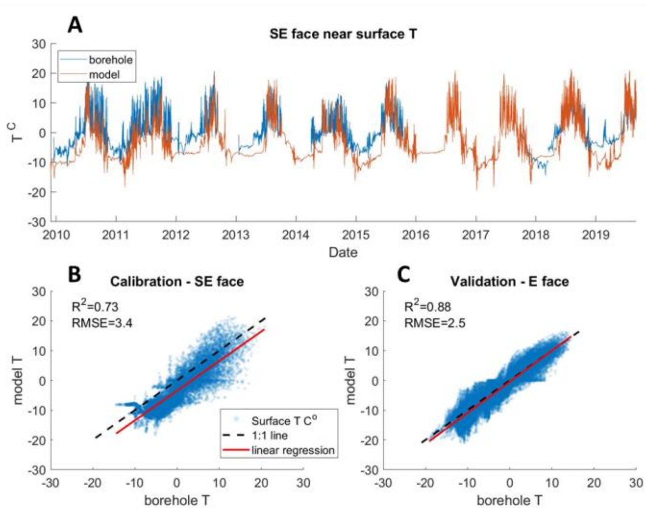

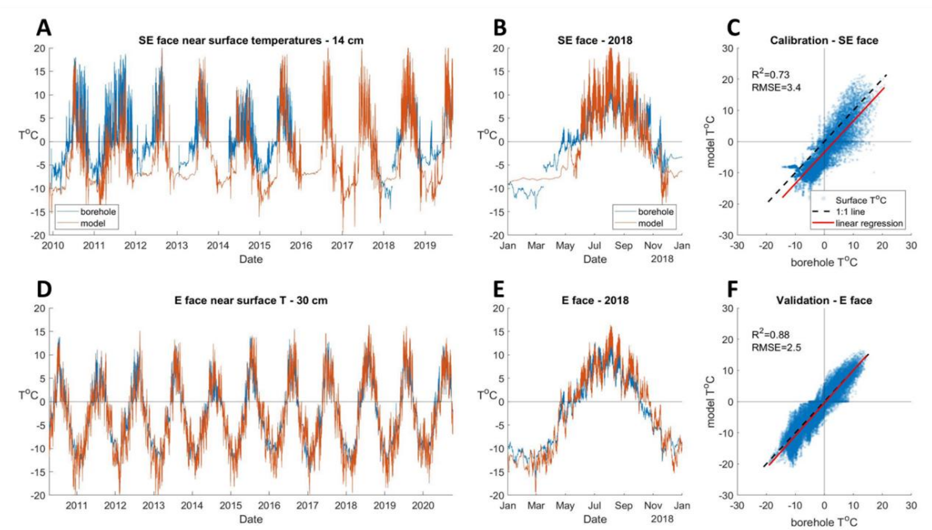

Figure 3: Comparison of near-surface temperature (T) data from model output and borehole measurements - A) Comparison of modeled near-surface ~~T~~temperature (orange) at depth 0.~~3~~14 m, with borehole measurement from the SE face study site (blue). ~~B)~~ B) Same as A showing modeled and observed rock temperatures during the year 2018. C) Correlation of modeled near-surface temperature (depth=0.~~3~~14 m) ~~as a function of~~and borehole temperature, SE face, after calibration of ~~snow fraction~~snowfall multiplication factor (0.25) and maximum snow depth (0.8 m). ~~C~~D) Comparison of modeled near-surface temperature (orange) at depth 0.30 m, with borehole measurement from the E face study site (blue). E) Same as D showing modeled and observed rock temperatures during the year 2018 F) Validating the modeled near~~-surface T at depth 0.14 m, with near~~-surface ~~T~~temperature at a depth of 0.3 m, with near-surface temperature data from a second borehole on the E face of ~~AdM~~Aiguille du Midi.

3.4. Effective snowmelt

Snow density is commonly used as a proxy for snow permeability (Marsh, 2005). We defined a threshold density value at the base of the snowpack for which no infiltration occurs and an ice crust develops (*i.e.*, hydraulic conductivity = 0). Based on an empirical relation suggested by Sommerfeld and Rocchio (1993), we define a threshold density value of 0.4 g/cm^3 which corresponds to a permeability value in the range of 10^{-10} m^2~~ range. In~~. For comparison, the average dry snow density in our simulation is 0.24 g/cm^3 with a standard deviation of 0.08 g/cm^3. We thus define effective snowmelt as the volume of water that exceeds the snow ~~pores~~porosity field capacity during model time steps ~~at which the~~ provided that dry snow density at the base of the snowpack~~, at the rock-snow contact, is no greater than~~ does not exceed 0.4 g/cm^3. In the CryoGrid model, snow density is controlled by compaction, metamorphism, refreezing, and water retention processes (Vionnet et al., 2012). The model also accounts for the inputs of rainfall to the snowpack water balance~~. To estimate the total potential of water availability for infiltration, we combine the effective snowmelt with the amount of rainfall that falls during partial or no snow cover~~.

4 Results

4.1. Calibrated model of the SE face of ~~AdM~~Aiguille du Midi

The ~~optimization~~calibration process for maximal snow depth ~~and snow multiplication factor~~ in the SE study site resulted in ~~values~~a value of 0.8 m ~~and 0.25 respectively. The optimized maximum snow depth value that we found~~. It corresponds to what we observed in our snow depth time series from the time-lapse camera (~~see 3.2~~Fig. 4) and high-resolution snow depth survey (~~see 3.1). We found that the model results with the S2M-SAFRAN forcing dataset provide satisfying results when comparing the temporal variation of snow accumulation with field measurement from nearby sites at Aiguilles Rouges (R^2=0.52) and Refuge du Requin (R^2=0.49) (Fig. 4A).~~Fig. 2). Modeled rock surface ~~T~~temperature shows a good correlation with borehole data from the SE face of ~~AdM~~Aiguille du Midi (R^2=0.73) (Fig. 3B). The validation of the model by simulating snow accumulation and near-surface temperatures in an E facing slope and comparing them with ~~a second borehole located there~~field measurements confirmed that the model is flexible for use within the ~~AdM~~Aiguille du Midi region ~~and is not single site specific~~ (R^2=0.88) (Fig. 3C~~).~~

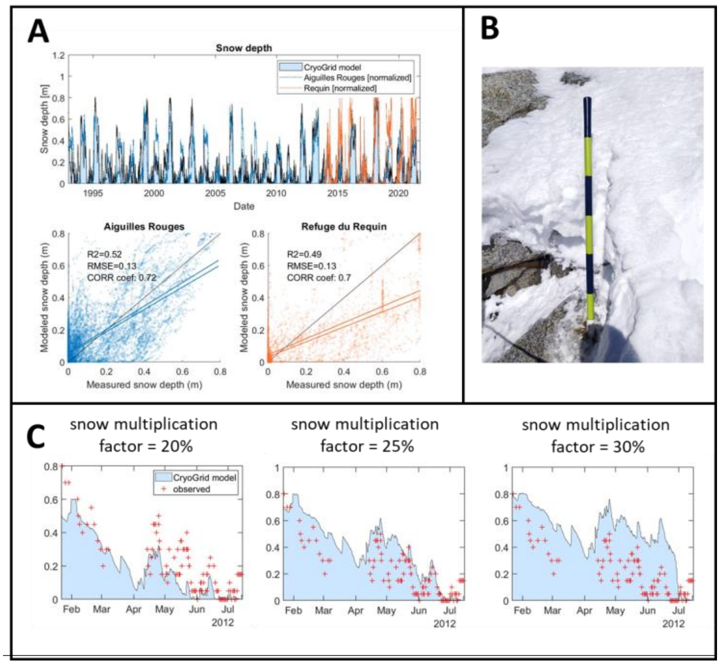

~~Figure : Comparison of modeled snow accumulation with field measurements - A) Comparison of modeled snow depth (black line + light blue area) with snow depth measurement in proximal stations (see Fig. 1 for locations) in the Mont-Blanc massif and its area: Aiguilles Rouges (blue) and Refuge du Requin (orange). Measurements were normalized to 0-0.8 m depth range for comparison. B) Snow depth pole installed~~, 4, supp. Fig. S4). The predictions of the near-surface rock temperatures on the E face were made with snow-free conditions and provided good correlation with field measurement (Fig. 3B). The reason for that is the location of the E borehole in a sub-vertical wall that does not accumulate snow and reduces much of the complexity of the surface energy balance calculations and the subsequent uncertainty.

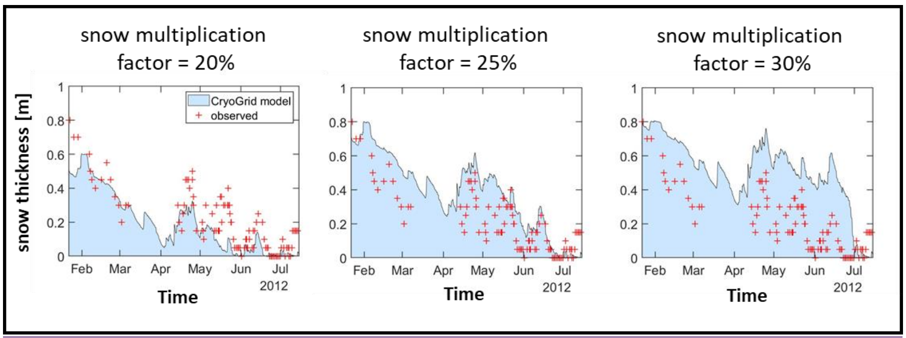

Figure 4~~SE facing rock slope to monitor snow depth time series with a time lapse camera. C)~~: Comparing modeled snow depth, under different ~~snow fraction~~snowfall multiplication factor values used in calibration, with measurements made in -situ using snow poles and a time-lapse camera. Note that using a multiplication factor of 0.2 (left) (20%) provides snow thickness values that are lower than the observed thickness (red cross) while a value of 0.3 (right) (30%) leads to higher than observed values. A multiplication factor value of 0.25 (25%) (middle) provides the optimum results~~ with snow fraction value of 0.25 (25% accumulation).~~.

4.2. Snow accumulation on steep rock walls

In the calibration process, we found that only about 25% of the snowfall accumulates on the steep rock slopes of our study site on the SE face of ~~AdM. The remaining 75% are likely redistributed by wind and gravity through avalanche and spindrift . We found that, for the E face, a snow fraction value of 10% improves the model results, suggesting that conditions are more prone to redistribution of the snowfall. This could be related to the fact the E face is on average 10º steeper than the SE face (average 55º vs. 65º~~Aiguille du Midi (See section 3.3.3 for more details).

Topographic analysis of the 10-cm-resolution survey of our field site shows a ~~heterogenous~~heterogeneous surface with local slope ranging between 20°-90° and a bimodal distribution with two well defined modes at 43° and 80° (Fig. 2D) which ~~illustrate~~illustrates the typical steep step-like rugged morphology of the SE rock slope. We resampled the topographic data to 1-m-resolution which is the realization dimension of our numerical model. We found that snow depth systematically decreases from a median depth of ~~70 cm~~0.7 m at a slope of 40° (~~and~~an average depth of ~~80 cm~~0.8 m) to <~~10 cm~~0.1 m at 70° slope. We thus use the value of ~~80 cm~~0.8 m as the maximum value of snow depth in our simulations. At lower slopes, between 25º- 40º, snow depth measurements ~~counter intuitively~~ show a counterintuitive positive correlation. Wirz et al. (2011) reported a similar trend in low slope angles and suggested that it is related to the relatively small area represented. In our case, cells with slope ~~<~~angles below 40° cover ~22% of the surface, and cells with slope <30º cover ~ only 6%. Many of the cells with slope <40° are located at a step edge where the ~~snow pack~~snowpack is not supported down slope and accumulation is thus relatively thin.

4.3. Snowmelt and water availability for infiltration

Figure 5 shows the SE face model results for annual amounts of ~~total~~net snowmelt, effective snowmelt (when the rock surface is penetrable and no ice crust exists at the base of the snowpack ~~bottom~~), direct rainfall (that falls ~~during times of no or partial~~on snow ~~cover~~-free area), and sublimation in the SE face of ~~AdM.~~Aiguille du Midi. All water fluxes are reported in length units of m (i.e. water equivalent of volume per area - m^3/m^2). We found that most of the annual water mass loss from the snowpack is the result of sublimation (Fig. 5A), ~~especially since sublimation~~which is the only process of snowpack mass loss during winter and spring months, from November to April ~~at~~, in our study site (Fig. 6). Average annual amount of net snowmelt is 0.13 m with ~~a~~ variability that ranges over a factor of six between 0.05-0.28 m, and is directly related to the annual amount of snow accumulation – years with relatively heavy snowfall will get more ~~total~~net snowmelt (Fig. 5B). The annual effective snowmelt ranges between ~~low~~ values ~~of~~below 0.~~014~~01 m (during the years ~~1968, 1990, 1992~~1977, 1984, 2000, 2007, 2011) and ~~highest values of~~ 0.~~11~~075-0.~~12~~1 m (during the years 1964, 1973, ~~1975, 1996, 2014~~1980, 1992). The fraction of effective snowmelt from the total annual excess water (effective snowmelt + runoff + direct rainfall) varies widely from 7 to 90% (during the years 1968 and 1975 respectively).

A

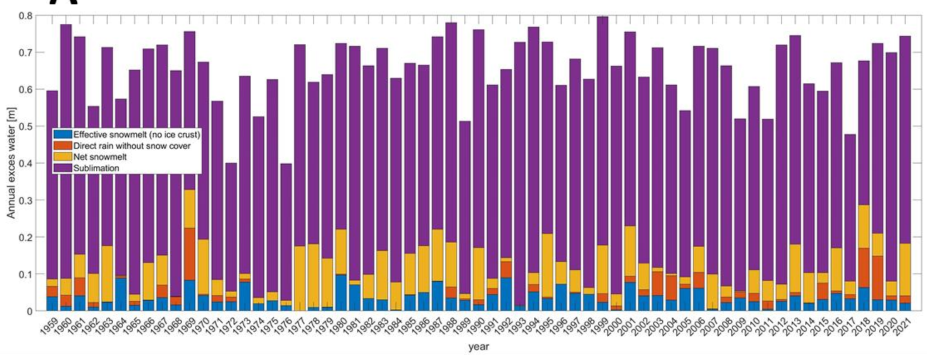
Effective snowmelt (no ice crust)
Direct rain without snow cover
Net snowmelt
Sublimation
Annual exces water [m]
year

B

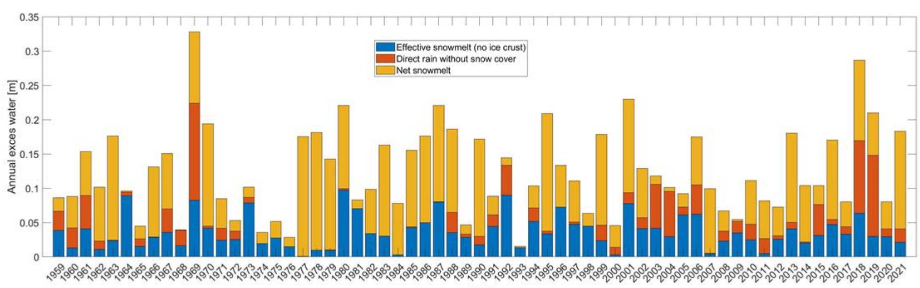
Effective snowmelt (no ice crust)
Direct rain without snow cover
Net snowmelt
Annual exces water [m]
year

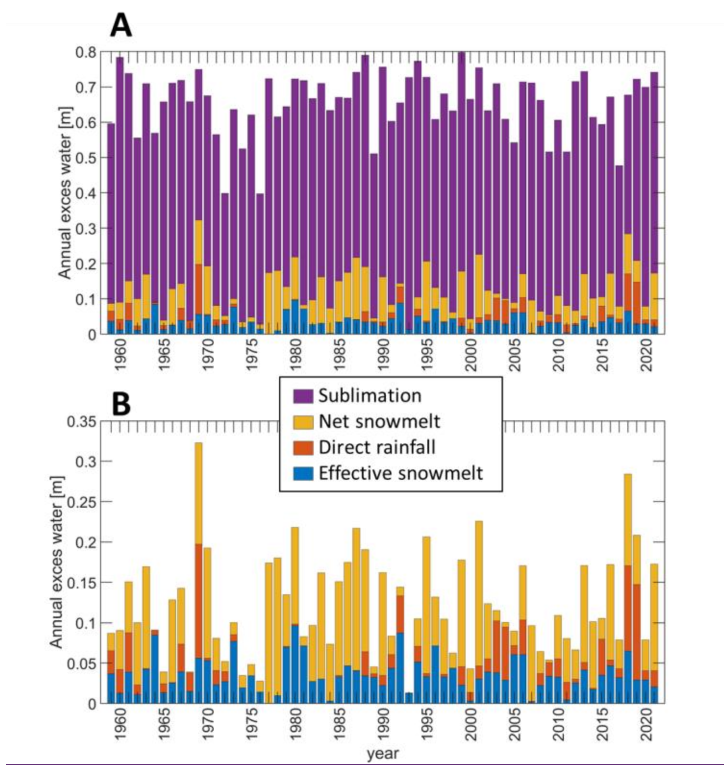

Figure 5: Annual water fluxes in the SE face study site between 1959-2020 - Model results of annual effective snowmelt (blue), direct rain (red), ~~total~~net snowmelt (yellow~~)~~), and sublimation (purple) in the SE face study site at 3800 m a.s.l. A) Water balance including sublimation. B) Total and effective snowmelt and direct rainfall. Note the high variability in annual water availability for infiltration (effective snowmelt + direct rain), and the high rate of sublimation~~ (bottom image).~~.

On average, ~~in~~at our study site on the SE face, 95% of the snowmelt ~~occur~~occurs from May to September; however, the effective snowmelt is delayed to the summer months (June to September) when ~~on average~~ 95% of the effective snowmelt occurs on average (Fig. 6). In most years, effective snowmelt begins in June or July. A few exceptional years show considerable effective snowmelt values in May (~~1974,~~ 1992, ~~1996,~~ 2017,2 018) and some show the first effective snowmelt only in August (~~1980 and~~1978, 1997, 2007, 2011). In all years, ~~>~~more than 90% of the effective ~~snow~~snowmelt is produced by the end of September.

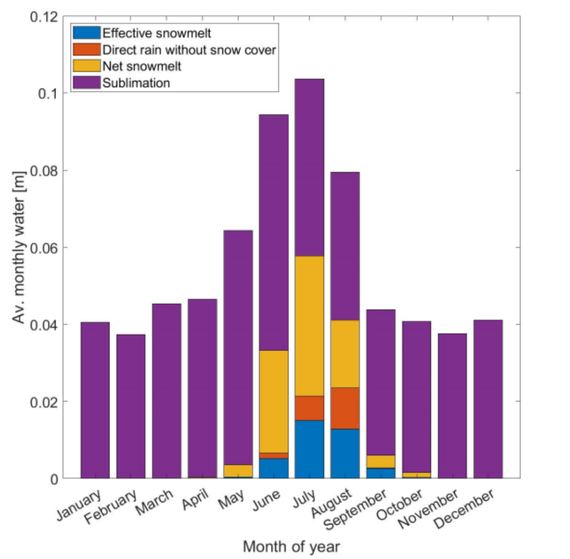

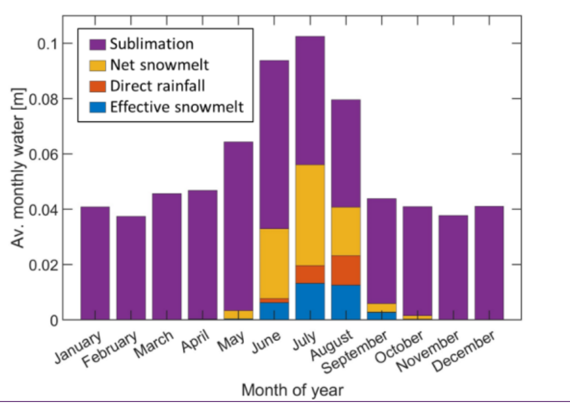

Figure 6: Average modeled monthly water fluxes in the SE study site for the period 1959-2020.

The flexibility of the model setup enables the simulation of opposite north and south facing rock slopes to test the effect of topographic aspect on runoff regime. ~~Model~~In these simulations we kept all model parameters identical and changes only the slope aspect direction. The results show that both north and south facing rock slopes experience complete melting of snow cover by late summer, which ~~is in agreement~~agrees with field observations~~.~~ (Fig. 7). Similar volumes of total runoff are produced, with negligible differences due to different sublimation rates. Interestingly, the annual effective snowmelt on south facing rock slopes is 48% greater on average than on north facing slopes (Fig. 7). The ~~reason~~reasons for this ~~is twofold: first, while the duration of~~are that effective snowmelt occurs from May to October on south facing rock-slopes~~ ranges from May to October, the effective snowmelt on the north face is limited to~~, while it takes place only from June to September ~~(fig. 7). This is related to the limited duration of the positive rock surface T on the north aspect~~on north facing slopes (Fig. 7~~)~~), and ~~the~~with longer persistence of ice crust at the base of the snowpack.

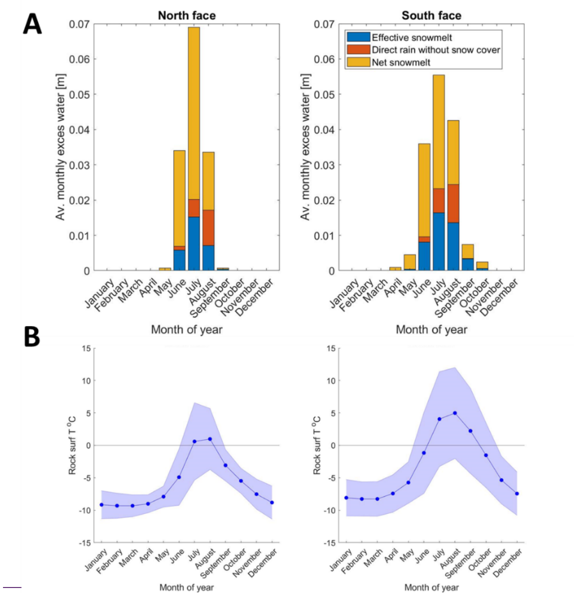
A
North face
South face
Effective snowmelt
Direct rain without snow cover
Net snowmelt
Av. monthly exces water [m]
Month of year
B
Rock surf T °C
Month of year

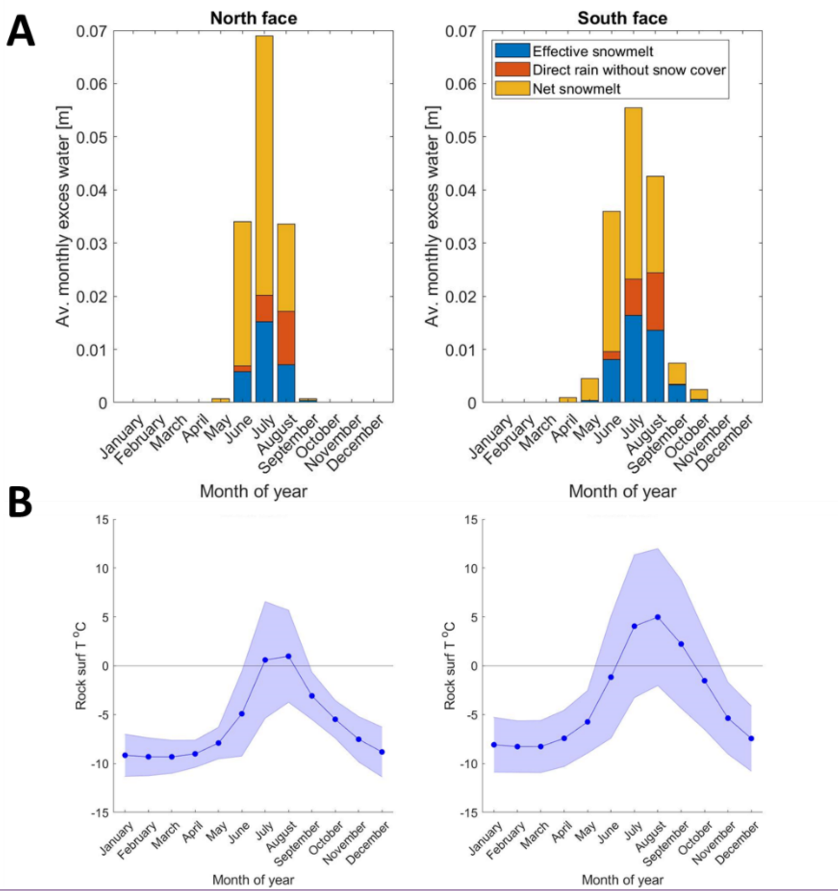

Figure 7: North vs. South comparison - A) Comparison of average monthly distribution of water fluxes in north and south facing rock slopes at an elevation of 3900 m a.s.l. Note that the annual effective snowmelt on south facing rock slopes is 48% greater on average than on north facing slopes~~, while the duration of effective snowmelt on south facing rock-slopes range from May to October, the effective snowmelt on the north face is limited to June to September.~~. B) Average surface temperature (T) in north and south facing rock slopes at an elevation of 3900 m a.s.l. Blue ~~area~~shading shows the standard deviation of monthly surface ~~T~~temperatures.

4.4. Modeling ~~elevation change~~energy and water balance at various altitudes

The S2M-SAFRAN dataset for the Mont-Blanc massif is available at elevation steps of 300 m. We compared our model simulation results for the ~~AdM~~Aiguille du Midi SE face with the same settings at ~~elevations of~~different altitudes, starting from 2700~~, 3000, 3300, 3600, 3900, 4200, 4500~~ m a.s.l, which is the elevation where discontinuous rock wall permafrost is expected to exist, and up to 4800 m a.s.l~~.~~, which is the highest point in the Mont-Blanc massif. These simulations give a better understanding of the thermal dynamics along the entire permafrost-affected mountain flank and the changes in effective snowmelt and water availability for infiltration. To broaden the analysis, we also modeled the effect of elevation change on a north facing slope. Our results show that for south facing rock slopes, snowmelt is the main source of water for infiltration in elevations above 3600 m a.s.l. From 3600 m to 2700 m, direct input of rainfall and ~~total~~net snowmelt volumes increase rapidly, while the effective snowmelt ~~increase~~increases at a more gradual rate (Fig. 8). At these lower elevations, where direct rainfall is dominant, effective snowmelt input precedes rainfall by ~1 month on average (Fig. 8A). Above 3300 m, sublimation is the dominant process of snow mass loss. The availability of water for infiltration, either by snowmelt or direct rainfall, occurs sooner at lower elevations~~. Above 3600 m,~~: water is available for infiltration ~~in June and~~ as early as April at ~~elevation~~elevations of 2700~~ – 3000 m~~-3000m, while the onset of snowmelt occurs in June at 3600m. A comparison with the same elevations on a north face (Fig. 9) shows that at elevations <3000 m, fluxes are similar~~ on both aspects.~~. At higher elevations, the ratio of water availability between north ~~to~~and south increases while the water fluxes magnitudes decrease.

A

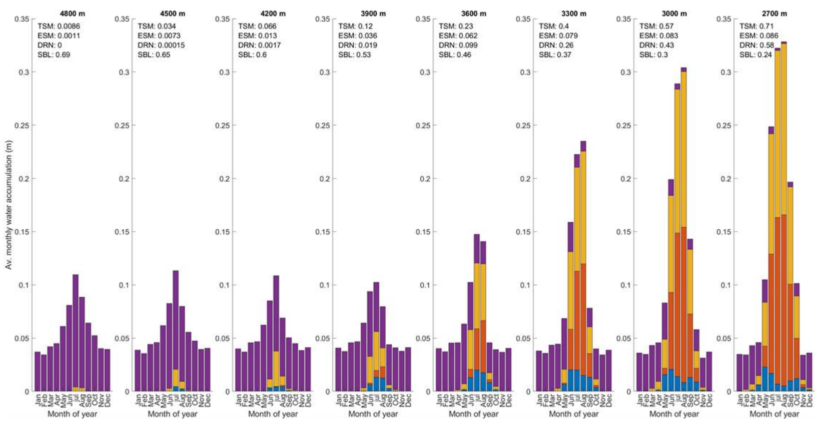
4800 m
TSM: 0.0086
ESM: 0.0011
DRN: 0
SBL: 0.69
4500 m
TSM: 0.034
ESM: 0.0073
DRN: 0.00015
SBL: 0.65
4200 m
TSM: 0.066
ESM: 0.013
DRN: 0.0017
SBL: 0.6
3900 m
TSM: 0.12
ESM: 0.036
DRN: 0.019
SBL: 0.53
3600 m
TSM: 0.23
ESM: 0.062
DRN: 0.099
SBL: 0.46
3300 m
TSM: 0.4
ESM: 0.079
DRN: 0.26
SBL: 0.37
3000 m
TSM: 0.57
ESM: 0.083
DRN: 0.43
SBL: 0.3
2700 m
TSM: 0.71
ESM: 0.086
DRN: 0.58
SBL: 0.24
Av. monthly water accumulation (m)
Month of year

B

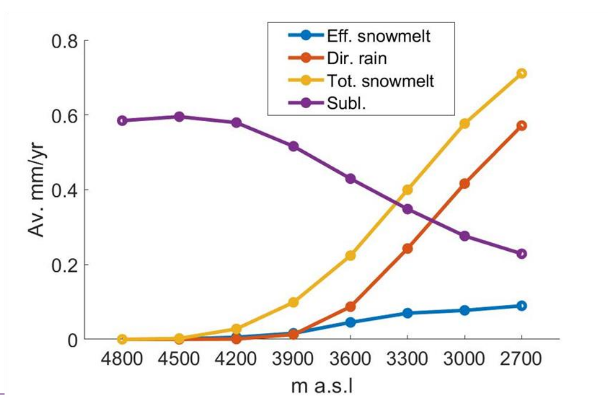
Eff. snowmelt
Dir. rain
Tot. snowmelt
Subl.
Av. mm/yr
0.8
0.6
0.4
0.2
0
4800 4500 4200 3900 3600 3300 3000 2700
m a.s.l

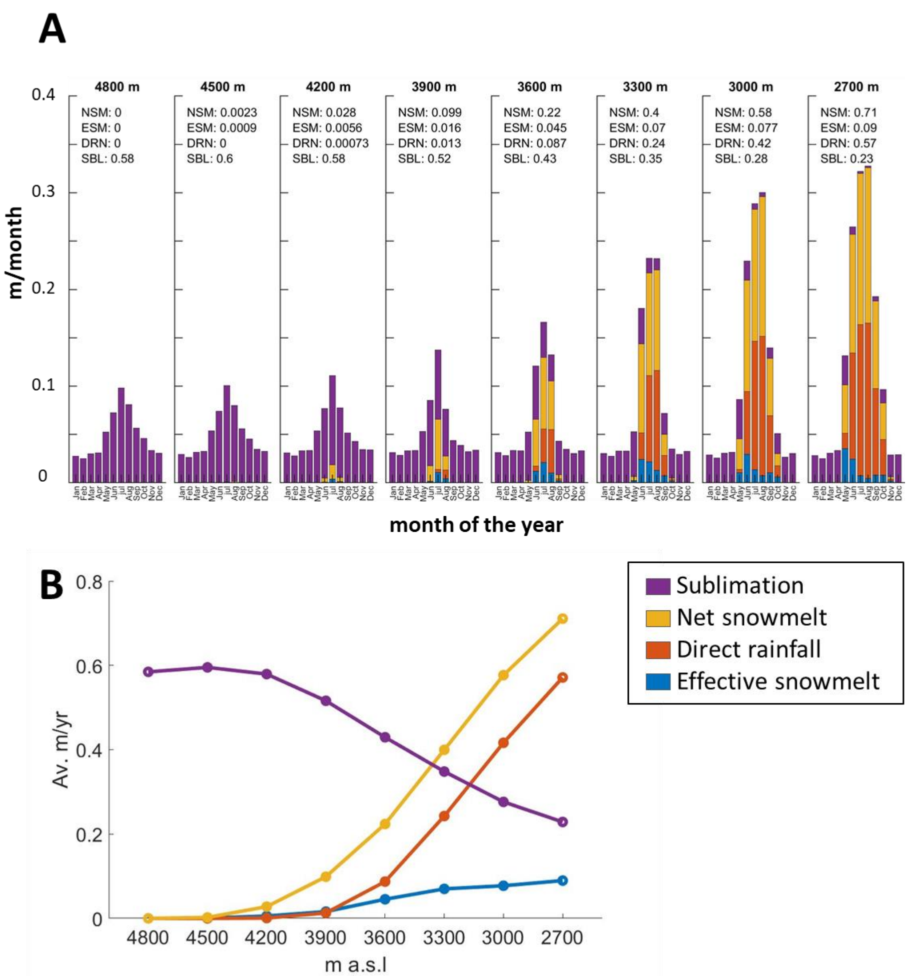

Figure 8: Comparison of average monthly distribution of water fluxes at elevations ranging from 4800 to 2700 m a.s.l. - A) Comparison of average monthly distribution of water fluxes, at conditions in elevations ~~of 4800,~~ 2700, 3000, 3300, 3600, 3900, 4200, 4500, ~~4200, 3900, 3600, 3300, 3000~~ and ~~2700~~4800 m a.s.l. based on the SE facing rock slope~~. TSM: total~~ calibrated model. NSM: net snowmelt; ESM: effective snowmelt; DRN: direct rainfall; SBL: sublimation. B) Average annual fluxes in each of the modeled elevations between 2700-4800~~-2700~~ m a.s.l. on SE facing rock slopes. Note the rapid increase in water availability from rainfall input below 3900 m.

5 Discussion

5.1. Snow **accumulation** depth

~~Our results show~~The spatial variability of snow depth in our study site shows a robust inverse relation between slope angle and snow accumulation depth, ~~which~~as mean snow depth decreases from 0.8 m to 0 m when slope angle increased from 45° to 75°. This observation is in agreement with the results of previous studies (Sommer et al., 2015; Blöschl et al., 1991; Winstral et al., 2002; Gruber Schmid and Sardemann, 2003; Haberkorn et al., 2015). The results also suggest that only 25% of the snowfall in the study site accumulates. The remaining 75%are likely redistributed by wind and gravity through avalanches and spindrifts (*e.g.* Hood and Hayashi, 2010). We acknowledge the observed variance in snow accumulation depth for a given slope (Fig. 2). This variance is interesting by itself since it might point to additional environmental factors that control snow accumulation, most likely local micro-topographic and micro-climatic factors (Wirz et al., 2011; Lehning et al., 2011). For example, the micro-topography of the rock surface can influence local wind dynamics and snow redistribution (Winstral et al., 2002). The rock slope roughness can affect friction with the snowpack surface and support its stability. Local shading can affect the thermal regime and mechanical characteristics of the snowpack (Vionnet et al., 2012). Further research using higher temporal (i.e. several per year) and spatial resolution (i.e. at a scale of surface roughness that is relevant for rock-snow friction) is needed to decipher the influence of slope characteristics other than slope angle on snow accumulation in steep slopes.

5.2. Model applications and flexibility of the S2M-SAFRAN dataset

~~On-site meteorological measurements in high mountain environments are difficult to setup and maintain and data is often discontinuous and limited. Remote sensing data from satellites and global climate models can be used to produce local climatic time series, however their spatial resolution is insufficient for rock slope scale processes.~~ We show that the use of the S2M-SAFRAN meteorological dataset can overcome some of ~~these~~the limitations~~, especially in locations where an *in-situ* meteorological stations is available nearby to improve its accuracy. Once calibrated, the CryoGrid model can benefit from the resolution~~ of ~~the S2M-SAFRAN data that is divided into elevation steps of 300 m.~~meteorological field measurements. The S2M-SAFRAN data is available for other mountain ranges in the Alps, Pyrenees (*e.g.* López-Moreno et al., 2020) and Corsica and our approach could be extended if enough field data is available for validation (*i.e.*, surface ~~T~~temperature and/or snow depth).

We show that the CryoGrid community model is a useful tool for studying near surface thermal and hydrological processes in steep mountainous ~~landscape~~landscapes. However, although the model allows considerations of lateral drainage, it is spatially limited to ~~one-dimensional~~1D configuration and ~~over simplify~~oversimplifies 3D subsurface thermal and hydrological processes. 3D hydrogeological models that can account for lateral flow, heat advection, and various saturation levels do exist. However, these models, in addition to often being closed sourced and costly, rarely include modules for simulating the complex processes in the snowpack and the interactions with meteorological and topographical conditions. We thus suggest that a complete model of the thermal and hydrological processes in mountainous periglacial and/or permafrost-affected landscapes can benefit from a coupling of the output of an energy balance ~~+~~plus snow hydrology model, such as CryoGrid, with a 3D hydrogeological model of mass and heat transfer.

5.3. Potential snowmelt and water balance

~~Our~~The results presented here are from a first attempt to fill a major knowledge gap in the field of ~~steep~~ mountain ~~slopes with~~ permafrost ~~related to~~hydrology and provide a constraint on one of the most important parameters - the availability of water for infiltration. We demonstrate ~~some of the known complexity~~previously suggested control of ~~the environmental controls~~snow hydrology on water availability in high-elevation steep rock slopes, ~~such as~~via the formation of an ice crust layer that can profoundly lower the local rock surface infiltration capacity (Woo and Heron, 1981; Woo et al., 1982; Marsh, 2005; Phillips et al., 2016). ~~We~~Our approach to simulating the formation of the ice crust and its influence on snow hydrology is likely oversimplified and ignores possible lateral fluxes and the formation of impermeable layers in the upper parts of the snowpack. Sublimation was found ~~sublimation~~ to be the ~~most~~ dominant process of snowpack mass loss~~.~~ in the field site at elevations higher than 3600 m a.s.l (excluding mass removal by wind and gravity). Accurate modeling of sublimation in steep~~–~~-high alpine terrain is highly complex and field measurements are rare, however, previous studies pointed out the importance of sublimation in the alpine snowpack mass balance, and thus in agreement with our model results (Strasser et al., 2008; MacDonald et al., 2010). We found sublimation rate to be sensitive to surface roughness length – a parameter that describes the efficiency of energy transfer (*i.e.* latent heat of sublimation) ~~between~~at the air~~ and the ~~-snowpack ~~surface~~interface. We tested the sensitivity of sublimation rates to a wide range of roughness ~~length (Table 1)~~lengths values (1×10^{-4} - 2×10^{-2} m, Table 2) and found that ~~and~~ although sublimation rate changed significantly, it remained the most dominant ~~flux~~process of snow mass loss. We show that effective snowmelt is the main source of water availability to the rock surface in steep high elevated rock slopes and that at ~~intermediate~~some elevations, *i.e.* 3600-3900 m a.s.l in our case study, a transition occurs from snowmelt-dominated to rainfall-dominated water availability (Fig. 8). A high rockfall frequency in such a permafrost-affected ~~site~~elevation range was recently demonstrated by Mourey et al. (2022) in the Mont-Blanc massif in the Grand Couloir du Goûter site, at elevations of 3300-3800 m a.s.l. We compared the influence of elevation on water balance in N and S facing hillslopes (Fig. 9A) and found that differences are more prominent at higher elevations – as S facing rock slopes receive more water input in ~~compare~~comparison with N facing (Fig. 9B). This results from the interplay of snow cover dynamics which in turn influence snowmelt and rock surface exposure to direct rain, in addition to differences in ice crust formation. Considering the connectivity in the slope length scale, some of the surface runoff that is generated from snowmelt at high elevation in spring and early summer, due to sealing of the rock surface with an ice crust, may reach a lower elevation where the rock is not sealed and amplify the observed increase in water contribution at the transition elevation.

In this contribution, we focus on the availability of water for infiltration at the rock surface; however, the actual infiltration rate depends on the infiltration capacity of the ~~rock.~~bulk rock, including pores and fractures. Any water fluxes that exceed the infiltration capacity will not infiltrate and flow as runoff. Maréchal et al. (1999) estimated the hydraulic conductivity of the bulk crystalline rock that composes the ~~AdM~~Aiguille du Midi to 10^{-8} m/s. Since the hydraulic conductivity of the granitic rock is much lower (Bear, 1988), the actual value is controlled by the fractures in the rock – their density, aperture and connectivity. Utilizing an empirical equation (Eq. 3) suggested by Kiraly (1969, 1994)~~ which accounts for~~:

$$k = \frac{g \cdot d^3 \cdot f}{12v} \qquad (3)$$

where k is the hydraulic conductivity (m/s), g is gravity acceleration (9.81 m/s^2), v is kinematic viscosity of water (3.2×10^{-6} m^2/s), d is average aperture of planar fissures (m), and f is average fracture ~~density and aperture,~~frequency (m^{-1}), and using conservative values of fracture density of 2 m^{-1} and fracture aperture of 0.5 mm, we get a value that is two orders of magnitude higher (6×10^{-6} m/s) than that of Maréchal et al. (1999)~~. Looking at our results,~~. If we convert our model results of effective snowmelt to the common units for hydraulic conductivity of m/s we find that 95% of the effective snowmelt ~~occur~~occurs at rates that fall between these estimations (10×10^{-8} - 6×10^{-6} m/s), thus making infiltration capacity (or hydraulic conductivity) an important parameter for estimation of infiltration in steep fractured rock ~~wall~~walls.

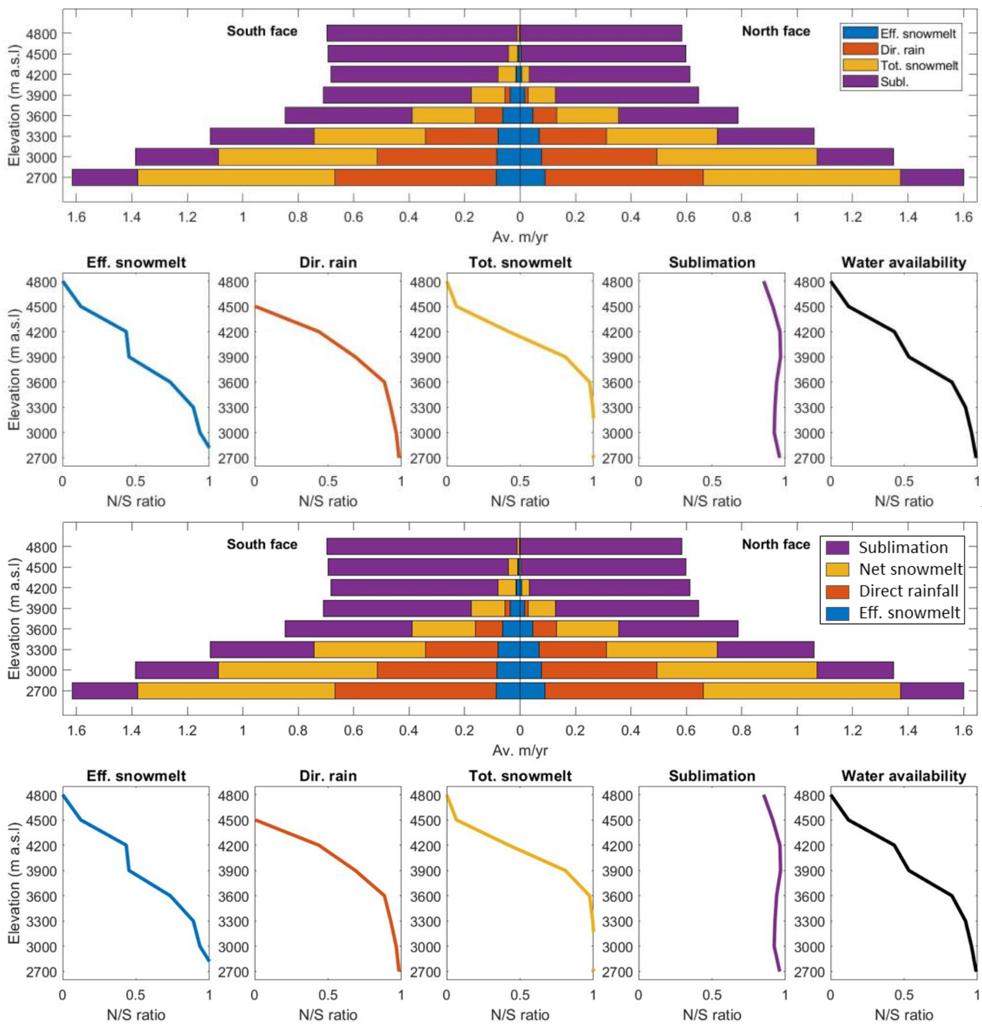

Figure 9: North vs. South comparison of average monthly distribution of water fluxes at elevations of 2700 – 4800 m a.s.l. – Top: Comparison of average annual water fluxes, at elevations of 4800, 4500, 4200, 3900, 3600, 3300, 3000 and 2700 m a.s.l. on north (left) and south (right) facing rock slopes. Bottom: The ratio between north to south of each component of the water fluxes described above, in each of the modeled elevation. A value of 1 represents equal flux on both aspects, and values decreasing toward 0 represent larger ratio between S to N face (for example, a value of 0.5 corresponds to ×2 higher flux on the S face). The bottom right image

shows the flux of net water availability at the rock surface, that is available for infiltration (effective snowmelt + direct rain). Note that at elevations <3000 m a.s.l fluxes are similar on both aspects and the ratio decreases at higher elevations but the water fluxes magnitudes decrease.

5.4. Implications of results

The new information we present on the timing and quantity of water input at the rock surface (Fig. 5, 6) can be used to improve the understanding of thermal, hydrogeological, and mechanical processes in steep mountain rock slopes, such as water pressure (Matsuoka, 2019; D'Amato et al., 2016) and ~~permafrost degradation that was previously shown to be linked with a~~ decrease in the mechanical stability of ~~steep~~ rock ~~slopes and initiation failure and rock fall occurrence~~ walls due to permafrost degradation (Gruber et al., 2004; Gruber and Haeberli, 2007; Ravanel and Deline, 2015).

Our model setup using the CryoGrid community model can be applied in other steep alpine rock slopes to assess water availability and ~~risk assessments from~~improve the understanding of thawing related rock failure.

We hypothesize that rock slopes at elevations of 3600-3900 m a.s.l., where we observe a sharp transition in water availability (Fig. 8), are especially sensitive to climate change. Our simulations show that water availability increases rapidly below these elevations due to high rates of direct rainfall. In a scenario ~~that~~of increasing air ~~temperatures~~temperature and ~~the intensity of~~ summer rains ~~increases~~intensity due to climate change (Pepin et al., 2022; Pepin et al., 2015)~~, and~~, the observed nonlinear trend of water input ~~is 'shifted'~~may shift upwards to higher elevations~~, we~~. We thus expect that higher-elevation permafrost-affected slopes will experience an abrupt increase in water input from rainfall which could prompt permafrost degradation and mechanical destabilization. This effect will be more prominent at the transition elevations that will change from snowmelt- to rainfall-dominated input, and less in higher elevations that will remain snowmelt-dominated. Field observations support this hypothesis: topographic analysis of data from 209 rockfalls in the Mont-Blanc massif between 2007 and 2015 (Legay et al., 2021) show that rockfalls on S, E and W facing rock walls ~~occur~~occurred mostly at ~~elevation~~elevations of 3300-3600 m, and at ~~elevation~~elevations of 3000-3300 m a.s.l on N facing rock walls (Fig. 10), suggesting that elevation dependent climate change is responsible for the observed peak in rockfalls occurrence at the water availability transition elevation (Pepin et al., 2022; Pepin et al., 2015)~~. During the 2003 and 2015 summer heatwaves in the Mont-Blanc massif,~~. Ravanel et al. (2017) showed that during the 2003 and 2015 summer heatwaves in the Mont-Blanc massif, numerous rock falls were initiated at average elevations of 3300 m a.s.l and 3600 m a.s.l on the north and south faces ~~respectfully,~~respectively and that ~~hydrostatic pressure related to thaw or extreme rain,~~thawing and ~~advective heat transport at depth by~~ water percolation along discontinuities are the likely rockfall triggering factors. The lower elevation of the maximum rockfall occurrence on the north face could also be related to the ~~influence of the lower snowline and related processes which are not accounted in the simplified aspect conversion of our model. 3600 m a.s.l. was also reported as the~~ lower boundary of ~~continuous stable~~ permafrost occurrence of ~~permafrost~~ in the Mont-Blanc massif (Magnin et al., 2015a)~~. Below 3600 m rockwall permafrost was shown to occur locally from an elevation of 1900 m a.s.l with strong dependency on local structural settings and aspect~~. In addition, our results could be used in parameterization and forcing data in further modeling of subsurface hydrogeological processes and larger spatial scale analysis, and to study watershed hydrology in high mountain environments and the role of heat advection by water infiltration through rock fractures (Hasler et al., 2011; Magnin and Josnin, 2021)~~.~~.

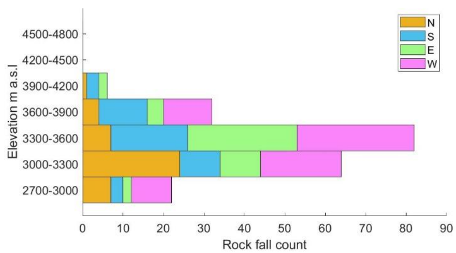

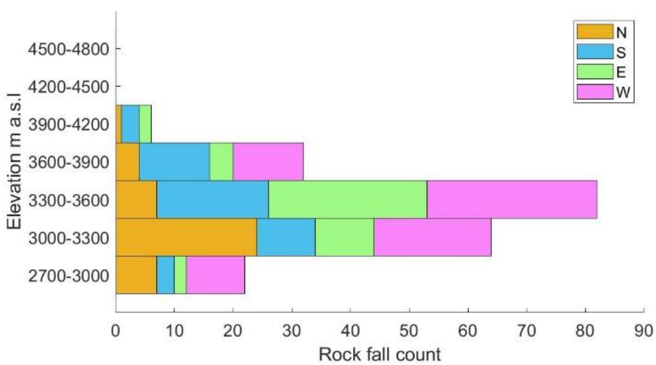

Figure 10: Topographic analysis of rockfalls documented by Legay et al. (2021) in the Mont-Blanc massif between 2007 and 2015. ~~Rock falls~~Rockfalls are most common at elevations of 3300-3600 m a.s.l. This trend is consistent for S, E and W facing slopes. On N facing slopes, the highest occurrence is at the elevation range of 3000-3300 m.

6 Conclusions

The importance of water in driving surface processes in steep periglacial landscapes is recognized by numerous studies. However, the complexity of the physical processes related to snow hydrology and challenges in data acquisition in these extreme environments result in a major knowledge gap in the availability of water at the slope surface. Using field ~~measurement~~measurements and numerical modeling, we simulated the energy balance and hydrological fluxes in a steep high-elevated permafrost-affected rock slope at a site in Aiguille du Midi~~,~~ (3842 m a.s.l), in the Mont-Blanc massif. We also applied the model to both north and south facing aspects and a range of elevations, between 2700 and 4800 m a.s.l, to study the effects of topography and micro-topography on water availability. Our results provide new ~~information about~~insights into water balance at the surface of steep rock slopes. This includes the quantity and temporal distribution of the effective snowmelt that is available for infiltration in addition to input from rainfall and mass losses by sublimation and runoff. Our results provide essential information to ~~risk assessments~~improve understanding of rock falls and rock avalanches that are ~~often~~sometimes thought to be triggered by water flow in fractures. We highlight the following conclusions:

- The combined application of the S2M-SAFRAN dataset with the CryoGrid community model ~~that we present here~~ is a powerful tool to study cryogenic and hydrologic processes in high alpine landscapes. Such capabilities are presented in this study in the comparison of various aspects, slope angles and elevations.
- We estimate that in our study site, in a steep rock slope on the SE face of ~~AdM~~Aiguille du Midi, only ~25% of the snowfall accumulates. The remaining ~75% is redistributed by wind and gravity. We also found that snow accumulation thickness is inversely correlated with surface slopes between 40° to 70°.
- Snowmelt occurs between late spring and ~~late summer~~early fall, and most of it does not reach the rock surface due to ~~a~~the formation of an impermeable ice layer at the base of the snowpack. The annual effective snowmelt that is available for infiltration is highly variable and ranges over a factor of six, between 0.05 and 0.28 m during the period 1959-2021. The ~~timing~~onset of ~~the first~~ effective snowmelt ~~in the year ranges~~occurs between May~~-~~ and August, and ~~effective snowmelt~~ ends before October; it precedes the first rainfall input by one month on average.
- Sublimation is the main process of snowpack mass loss in our study site.
- Results of model simulations at ~~varying~~various elevations show that effective snowmelt is the main source of potential water for infiltration at elevation >3600 m a.s.l. Below 3600 m, direct rainfall is becoming more dominant. The change from snowmelt-dominated to rainfall-dominated water availability is nonlinear and characterized by a rapid increase in water availability for infiltration. We suggest that this transition elevation is highly sensitive to climate change, as permafrost-affected slopes experience an abrupt increase in water input that can initiate rock failure.

Author contributions

~~MBA~~MB and FM conceptualized and designed the research. ~~MBA~~MB analyzed the data. ~~MBA~~MB, FM, JB, EM, JB performed ~~field work~~fieldwork. SW developed the model and wrote the code. ~~MBA~~MB, FM, SW, JB, ~~SW~~JB, LR and PD wrote the manuscript.

~~Acknowledgements~~Acknowledgments and data availability

This study is funded by the ANR-19-CE01-0018 WISPER project. We thank the Compagnie du Mont-Blanc and the Aiguille du Midi station staff for their support ~~in~~and access to the site. We are grateful to the two anonymous reviewers, whose comments allowed to significantly improve the manuscript.

Data used in this paper are available at https://zenodo.org/record/7224692#.Y0--OnaxWUk~~https://zenodo.org/record/7224692#.Y0--OnaxWUk~~. The S2M-SAFRAN reanalysis atmospheric data is available at https://www.aeris-data.fr/landing-page/?uuid=865730e8-edeb-4c6b-ae58-80f95166509b.

References

Allen, S. K., Gruber, S., and Owens, I. F.: Exploring steep bedrock permafrost and its relationship with recent slope failures in the Southern Alps of New Zealand, Permafr. Periglac. Process., 20, 345–356, https://doi.org/10.1002/ppp.658, 2009.

Bear, J.: Dynamics of Fluids in Porous Media, Courier Corporation, 806 pp., 1988.

Bertini, G., Marcucci, M., Nevini, R., Passerini, P., and Sguazzoni, G.: Patterns of faulting in the Mont Blanc granite, Tectonophysics, 111, 65–106, https://doi.org/10.1016/0040-1951(85)90066-6, 1985.

Blöschl, G., Kirnbauer, R., and Gutknecht, D.: Distributed Snowmelt Simulations in an Alpine Catchment: 1. Model Evaluation on the Basis of Snow Cover Patterns, Water Resour. Res., 27, 3171–3179, https://doi.org/10.1029/91WR02250, 1991.

Boeckli, L., Brenning, A., Gruber, S., and Noetzli, J.: Permafrost distribution in the European Alps: calculation and evaluation of an index map and summary statistics, The Cryosphere, 6, 807–820, https://doi.org/10.5194/tc-6-807-2012, 2012.

Boone, A. and Etchevers, P.: An Intercomparison of Three Snow Schemes of Varying Complexity Coupled to the Same Land Surface Model: Local-Scale Evaluation at an Alpine Site, J. Hydrometeorol., 2, 374–394, https://doi.org/10.1175/1525-7541(2001)002<0374:AIOTSS>2.0.CO;2, 2001.

Bussy, F. and Von Raumer, J.: U–Pb geochronology of Palaeozoic magmatic events in the Mont-Blanc Crystalline Massif, Western Alps, Schweiz. Mineral. Petrogr. Mitteilungen, 74, 514–515, 1994.

D'Amato, J., Hantz, D., Guerin, A., Jaboyedoff, M., Baillet, L., and Mariscal, A.: Influence of meteorological factors on rockfall occurrence in a middle mountain limestone cliff, Nat. Hazards Earth Syst. Sci., 16, 719–735, https://doi.org/10.5194/nhess-16-719-2016, 2016.

Draebing, D. and Krautblatter, M.: The Efficacy of Frost Weathering Processes in Alpine Rockwalls, Geophys. Res. Lett., 46, 6516–6524, https://doi.org/10.1029/2019GL081981, 2019.

Durand, Y., Brun, E., Merindol, L., Guyomarc'h, G., Lesaffre, B., and Martin, E.: A meteorological estimation of relevant parameters for snow models, Ann. Glaciol., 18, 65–71, https://doi.org/10.3189/S0260305500011277, 1993.

Dwivedi, R. D., Singh, P. K., Singh, T. N., and Singh, D. P.: Compressive strength and tensile strength of rocks at sub-zero temperature, Indian J. Eng. Mater. Sci., 5, 43–48, 1998.

Eppes, M. C. and Keanini, R.: Mechanical weathering and rock erosion by climate-dependent subcritical cracking, Rev. Geophys., 55, 470–508, https://doi.org/10.1002/2017RG000557, 2017.

Essel, B., McDonald, J., Bolger, M., and Cahalane, C.: INITIAL STUDY ASSESSING THE SUITABILITY OF DRONES WITH LOW-COST GNSS AND IMU FOR MAPPING OVER FEATURELESS TERRAIN USING DIRECT GEOREFERENCING, Int. Arch. Photogramm. Remote Sens. Spat. Inf. Sci., XLIII-B2-2022, 37–44, https://doi.org/10.5194/isprs-archives-XLIII-B2-2022-37-2022, 2022.

Evans, I. S.: An integrated system of terrain analysis and slope mapping, Z. Geomorphol., 36, 274–295, 1980.

Fierz, C., Armstrong, R. L., Durand, Y., Etchevers, P., Greene, E., Mcclung, D. M., Nishimura, K., Satyawali, P. K., and Sokratov, S. A.: The International Classification for Seasonal Snow on the Ground, UNESCO, Paris, 2009.

Fischer, L., Amann, F., Moore, J. R., and Huggel, C.: Assessment of periglacial slope stability for the 1988 Tschierva rock avalanche (Piz Morteratsch, Switzerland), Eng. Geol., 116, 32–43, https://doi.org/10.1016/j.enggeo.2010.07.005, 2010.

French, H. M.: The Periglacial Environment, https://doi.org/10.1002/9781119132820, 2017.

Gardent, M., Rabatel, A., Dedieu, J.-P., and Deline, P.: Multitemporal glacier inventory of the French Alps from the late 1960s to the late 2000s, Glob. Planet. Change, 120, 24–37, https://doi.org/10.1016/j.gloplacha.2014.05.004, 2014.

Gruber, S. and Haeberli, W.: Permafrost in steep bedrock slopes and its temperatures-related destabilization following climate change, J. Geophys. Res. Earth Surf., 112, 1–10, https://doi.org/10.1029/2006JF000547, 2007.

Gruber, S., Hoelzle, M., and Haeberli, W.: Rock-wall temperatures in the Alps: Modelling their topographic distribution and regional differences, Permafr. Periglac. Process., 15, 299–307, https://doi.org/10.1002/ppp.501, 2004.

Gruber Schmid, U. and Sardemann, S.: High-frequency avalanches: release area characteristics and run-out distances, Cold Reg. Sci. Technol., 37, 439–451, https://doi.org/10.1016/S0165-232X(03)00083-1, 2003.

Haberkorn, A., Phillips, M., Kenner, R., Rhyner, H., Bavay, M., Galos, S. P., and Hoelzle, M.: Thermal Regime of Rock and its Relation to Snow Cover in Steep Alpine Rock Walls: Gemsstock, Central Swiss Alps, Geogr. Ann. Ser. Phys. Geogr., 97, 579–597, https://doi.org/10.1111/geoa.12101, 2015.

Haberkorn, A., Wever, N., Hoelzle, M., Phillips, M., Kenner, R., Bavay, M., and Lehning, M.: Distributed snow and rock temperature modelling in steep rock walls using Alpine3D, Cryosphere, 11, 585–607, https://doi.org/10.5194/tc-11-585-2017, 2017.

Haeberli, W. and Gruber, S.: Global Warming and Mountain Permafrost, in: Permafrost Soils, vol. 16, edited by: Margesin, R., Springer Berlin Heidelberg, Berlin, Heidelberg, 205–218, https://doi.org/10.1007/978-3-540-69371-0_14, 2009.

Haeberli, W., Noetzli, J., Arenson, L., Delaloye, R., Gärtner-Roer, I., Gruber, S., Isaksen, K., Kneisel, C., Krautblatter, M., and Phillips, M.: Mountain permafrost: development and challenges of a young research field, J. Glaciol., 56, 1043–1058, https://doi.org/10.3189/002214311796406121, 2010.

Hasler, A., Gruber, S., Font, M., and Dubois, A.: Advective heat transport in frozen rock clefts: Conceptual model, laboratory experiments and numerical simulation, Permafr. Periglac. Process., 22, 378–389, https://doi.org/10.1002/ppp.737, 2011.

Hersbach, H., Bell, B., Berrisford, P., Hirahara, S., Horányi, A., Muñoz-Sabater, J., Nicolas, J., Peubey, C., Radu, R., Schepers, D., Simmons, A., Soci, C., Abdalla, S., Abellan, X., Balsamo, G., Bechtold, P., Biavati, G., Bidlot, J., Bonavita, M., Chiara, G., Dahlgren, P., Dee, D., Diamantakis, M., Dragani, R., Flemming, J., Forbes, R., Fuentes, M., Geer, A., Haimberger, L., Healy, S., Hogan, R. J., Hólm, E., Janisková, M., Keeley, S., Laloyaux, P., Lopez, P., Lupu, C., Radnoti, G., Rosnay, P., Rozum, I., Vamborg, F., Villaume, S., and Thépaut, J.: The ERA5 global reanalysis, Q. J. R. Meteorol. Soc., 146, 1999–2049, https://doi.org/10.1002/qj.3803, 2020.

Hood, J. L. and Hayashi, M.: Assessing the application of a laser rangefinder for determining snow depth in inaccessible alpine terrain, Hydrol. Earth Syst. Sci., 14, 901–910, https://doi.org/10.5194/hess-14-901-2010, 2010.

Huggel, C., Allen, S., Deline, P., Fischer, L., Noetzli, J., and Ravanel, L.: Ice thawing, mountains falling-are alpine rock slope failures increasing, Geol. Today, 28, 98–104, https://doi.org/10.1111/j.1365-2451.2012.00836.x, 2012.

Jain, K.: How Photogrammetric Software Works: A Perspective Based on UAV's Exterior Orientation Parameters, J. Indian Soc. Remote Sens., 49, 641–649, https://doi.org/10.1007/s12524-020-01256-8, 2021.

Kiraly, L.: Groundwater flow in fractured rocks: models and reality: with 15 figures (with author annotations), in: 14. Mintrop-Seminar über Interpretationsstrategien in Exploration und Produktion, 1–21, 1994.

Kiraly, Laszlo.: Anisotropie et hétérogénéité de la perméabilité dans les calcaires fissurés (Anisotropy and heterogeneity of permeability in fractured limestones), Eclogae Geol. Helvetiae, 62, 613–619, 1969.

Krautblatter, M., Funk, D., and Günzel, F. K.: Why permafrost rocks become unstable: A rock-ice-mechanical model in time and space, Earth Surf. Process. Landf., 38, 876–887, https://doi.org/10.1002/esp.3374, 2013.

Legay, A., Magnin, F., and Ravanel, L.: Rock temperature prior to failure: Analysis of 209 rockfall events in the Mont Blanc massif (Western European Alps), Permafr. Periglac. Process., 32, 520–536, https://doi.org/10.1002/ppp.2110, 2021.

Lehning, M., Grünewald, T., and Schirmer, M.: Mountain snow distribution governed by an altitudinal gradient and terrain roughness: ROUGHNESS CONTROL ON MOUNTAIN SNOW, Geophys. Res. Lett., 38, n/a-n/a, https://doi.org/10.1029/2011GL048927, 2011.

Leloup, P. H., Arnaud, N., Sobel, E. R., and Lacassin, R.: Alpine thermal and structural evolution of the highest external crystalline massif: The Mont Blanc: EXHUMATION OF THE MONT BLANC MASSIF, Tectonics, 24, n/a-n/a, https://doi.org/10.1029/2004TC001676, 2005.

Li, N., Zhang, P., Chen, Y., and Swoboda, G.: Fatigue properties of cracked, saturated and frozen sandstone samples under cyclic loading, Int. J. Rock Mech. Min. Sci., 40, 145–150, https://doi.org/10.1016/S1365-1609(02)00111-9, 2003.

López-Moreno, J. I., Soubeyroux, J. M., Gascoin, S., Alonso-Gonzalez, E., Durán-Gómez, N., Lafaysse, M., Vernay, M., Carmagnola, C., and Morin, S.: Long-term trends (1958–2017) in snow cover duration and depth in the Pyrenees, Int. J. Climatol., 40, 6122–6136, https://doi.org/10.1002/joc.6571, 2020.

MacDonald, M. K., Pomeroy, J. W., and Pietroniro, A.: On the importance of sublimation to an alpine snow mass balance in the Canadian Rocky Mountains, Hydrol. Earth Syst. Sci., 14, 1401–1415, https://doi.org/10.5194/hess-14-1401-2010, 2010.

Magnin, F. and Josnin, J.-Y.: Water Flows in Rockwall Permafrost : a Numerical Approach Coupling Hydrological and Thermal Processes, J. Geophys. Res. Earth Surf., 2021.

Magnin, F., Brenning, A., Bodin, X., Deline, P., and Ravanel, L.: Modélisation statistique de la distribution du permafrost de paroi : application au massif du Mont Blanc, Géomorphologie Relief Process. Environ., 21, 145–162, https://doi.org/10.4000/geomorphologie.10965, 2015a.

Magnin, F., Deline, P., Ravanel, L., Noetzli, J., and Pogliotti, P.: Thermal characteristics of permafrost in the steep alpine rock walls of the Aiguille du Midi (Mont Blanc Massif, 3842 m a.s.l), Cryosphere, 9, 109–121, https://doi.org/10.5194/tc-9-109-2015, 2015b.

Magnin, F., Westermann, S., Pogliotti, P., Ravanel, L., Deline, P., and Malet, E.: Snow control on active layer thickness in steep alpine rock walls (Aiguille du Midi, 3842 m a.s.l., Mont Blanc massif), Catena, 149, 648–662, https://doi.org/10.1016/j.catena.2016.06.006, 2017.

Mamot, P., Weber, S., Schröder, T., and Krautblatter, M.: A temperature- and stress-controlled failure criterion for ice-filled permafrost rock joints, The Cryosphere, 12, 3333–3353, https://doi.org/10.5194/tc-12-3333-2018, 2018.

Mamot, P., Weber, S., Lanz, M., and Krautblatter, M.: Brief communication: The influence of mica-rich rocks on the shear strength of ice-filled discontinuities, The Cryosphere, 14, 1849–1855, https://doi.org/10.5194/tc-14-1849-2020, 2020.

Maréchal, J. C., Perrochet, P., and Tacher, L.: Long-term simulations of thermal and hydraulic characteristics in a mountain massif: The Mont Blanc case study, French and Italian Alps, Hydrogeol. J., 7, 341–354, https://doi.org/10.1007/s100400050207, 1999.

Marsh, P.: Water Flow through Snow and Firn, in: Encyclopedia of Hydrological Sciences, edited by: Anderson, M. G. and McDonnell, J. J., John Wiley & Sons, Ltd, Chichester, UK, hsa167, https://doi.org/10.1002/0470848944.hsa167, 2005.

Matsuoka, N.: Frost weathering and rockwall erosion in the southeastern Swiss Alps: Long-term (1994-2006) observations, Geomorphology, 99, 353–368, https://doi.org/10.1016/j.geomorph.2007.11.013, 2008.

Matsuoka, N.: A multi-method monitoring of timing, magnitude and origin of rockfall activity in the Japanese Alps, Geomorphology, 336, 65–76, https://doi.org/10.1016/j.geomorph.2019.03.023, 2019.

Mellor, M.: Mechanical properties of rocks at low temperatures, in: 2nd International Conference on Permafrost, Yakutsk, International Permafrost Association, 334–344, 1973.

Mineo, S. and Pappalardo, G.: Rock Emissivity Measurement for Infrared Thermography Engineering Geological Applications, Appl. Sci., 11, 3773, https://doi.org/10.3390/app11093773, 2021.

Mott, R., Schirmer, M., Bavay, M., Grünewald, T., and Lehning, M.: Understanding snow-transport processes shaping the mountain snow-cover, Cryosphere, 4, 545–559, https://doi.org/10.5194/tc-4-545-2010, 2010.

Mourey, J., Lacroix, P., Duvillard, P.-A., Marsy, G., Marcer, M., Malet, E., and Ravanel, L.: Multi-method monitoring of rockfall activity along the classic route up Mont Blanc (4809 m a.s.l.) to encourage adaptation by mountaineers, Nat. Hazards Earth Syst. Sci., 22, 445–460, https://doi.org/10.5194/nhess-22-445-2022, 2022.

Myhra, K. S., Westermann, S., and Etzelmüller, B.: Modelled Distribution and Temporal Evolution of Permafrost in Steep Rock Walls Along a Latitudinal Transect in Norway by CryoGrid 2D, Permafr. Periglac. Process., 28, 172–182, https://doi.org/10.1002/ppp.1884, 2017.

Pepin, N. C., Bradley, R. S., Diaz, H. F., Baraer, M., Caceres, E. B., Forsythe, N., Fowler, H., Greenwood, G., Hashmi, M. Z., Liu, X. D., Miller, J. R., Ning, L., Ohmura, A., Palazzi, E., Rangwala, I., Schöner, W., Severskiy, I., Shahgedanova, M., Wang, M. B., Williamson, S. N., and Yang, D. Q.: Elevation-dependent warming in mountain regions of the world, Nat. Clim. Change, 5, 424–430, https://doi.org/10.1038/nclimate2563, 2015.

Pepin, N. C., Arnone, E., Gobiet, A., Haslinger, K., Kotlarski, S., Notarnicola, C., Palazzi, E., Seibert, P., Serafin, S., Schöner, W., Terzago, S., Thornton, J. M., Vuille, M., and Adler, C.: Climate Changes and Their Elevational Patterns in the Mountains of the World, Rev. Geophys., 60, https://doi.org/10.1029/2020RG000730, 2022.

Phillips, M., Haberkorn, A., Draebing, D., Krautblatter, M., Rhyner, H., and Kenner, R.: Seasonally intermittent water flow through deep fractures in an Alpine Rock Ridge: Gemsstock, Central Swiss Alps, Cold Reg. Sci. Technol., 125, 117–127, https://doi.org/10.1016/j.coldregions.2016.02.010, 2016.

Phillips, M., Haberkorn, A., and Rhyner, H.: Snowpack characteristics on steep frozen rock slopes, Cold Reg. Sci. Technol., 141, 54–65, https://doi.org/10.1016/j.coldregions.2017.05.010, 2017.

Rasmussen, R., Baker, B., Kochendorfer, J., Meyers, T., Landolt, S., Fischer, A. P., Black, J., Thériault, J. M., Kucera, P., Gochis, D., Smith, C., Nitu, R., Hall, M., Ikeda, K., and Gutmann, E.: How Well Are We Measuring Snow: The NOAA/FAA/NCAR Winter Precipitation Test Bed, Bull. Am. Meteorol. Soc., 93, 811–829, https://doi.org/10.1175/BAMS-D-11-00052.1, 2012.

Ravanel, L. and Deline, P.: Climate influence on rockfalls in high-alpine steep rockwalls: The north side of the aiguilles de chamonix (mont blanc massif) since the end of the “Little Ice Age,” Holocene, 21, 357–365, https://doi.org/10.1177/0959683610374887, 2011.

Ravanel, L. and Deline, P.: A network of observers in the Mont-Blanc massif to study rockfall from high Alpine rockwalls, Geogr. Fis. E Din. Quat., 151–158, https://doi.org/10.4461/GFDQ.2013.36.12, 2013.

Ravanel, L. and Deline, P.: Rockfall Hazard in the Mont Blanc Massif Increased by the Current Atmospheric Warming, in: Engineering Geology for Society and Territory - Volume 1, edited by: Lollino, G., Manconi, A., Clague, J., Shan, W., and Chiarle, M., Springer International Publishing, Cham, 425–428, https://doi.org/10.1007/978-3-319-09300-0_81, 2015.

Ravanel, L., Magnin, F., and Deline, P.: Impacts of the 2003 and 2015 summer heatwaves on permafrost-affected rock-walls in the Mont Blanc massif, Sci. Total Environ., 609, 132–143, https://doi.org/10.1016/j.scitotenv.2017.07.055, 2017.

Richards, L. A.: Capillary conduction of liquids through porous mediums, Physics, 1, 318–333, https://doi.org/10.1063/1.1745010, 1931.

Rossi, M., Rolland, Y., Vidal, O., and Cox, S. F.: Geochemical variations and element transfer during shear-zone development and related episyenites at middle crust depths: insights from the Mont Blanc granite (French — Italian Alps), Geol. Soc. Lond. Spec. Publ., 245, 373–396, https://doi.org/10.1144/GSL.SP.2005.245.01.18, 2005.

Schmidt, J. U., Etzelmüller, B., Schuler, T. V., Magnin, F., Boike, J., Langer, M., and Westermann, S.: Surface temperatures and their influence on the permafrost thermal regime in high-Arctic rock walls on Svalbard, Cryosphere, 15, 2491–2509, https://doi.org/10.5194/tc-15-2491-2021, 2021.

Sokratov, S. A. and Sato, A.: The effect of wind on the snow cover, Ann. Glaciol., 32, 116–120, https://doi.org/10.3189/172756401781819436, 2001.

Sommer, C. G., Lehning, M., and Mott, R.: Snow in a Very Steep Rock Face: Accumulation and Redistribution During and After a Snowfall Event, Front. Earth Sci., 3, https://doi.org/10.3389/feart.2015.00073, 2015.

Sommerfeld, R. A. and Rocchio, J. E.: Permeability measurements on new and equitemperature snow, Water Resour. Res., 29, 2485–2490, https://doi.org/10.1029/93WR01071, 1993.

Strasser, U., Bernhardt, M., Weber, M., Liston, G. E., and Mauser, W.: Is snow sublimation important in the alpine water balance?, The Cryosphere, 2, 53–66, https://doi.org/10.5194/tc-2-53-2008, 2008.

Tonkin, T. N., Midgley, N. G., Cook, S. J., and Graham, D. J.: Ice-cored moraine degradation mapped and quantified using an unmanned aerial vehicle: A case study from a polythermal glacier in Svalbard, Geomorphology, 258, 1–10, https://doi.org/10.1016/j.geomorph.2015.12.019, 2016.

Vernay, M., Lafaysse, M., Monteiro, D., Hagenmuller, P., Nheili, R., Samacoïts, R., Verfaillie, D., and Morin, S.: The S2M meteorological and snow cover reanalysis over the French mountainous areas: description and evaluation (1958–2021), Earth Syst. Sci. Data, 14, 1707–1733, https://doi.org/10.5194/essd-14-1707-2022, 2022.

Vionnet, V., Brun, E., Morin, S., Boone, A., Faroux, S., Le Moigne, P., Martin, E., and Willemet, J.-M.: The detailed snowpack scheme Crocus and its implementation in SURFEX v7.2, Geosci. Model Dev., 5, 773–791, https://doi.org/10.5194/gmd-5-773-2012, 2012.

Vivero, S. and Lambiel, C.: Monitoring the crisis of a rock glacier with repeated UAV surveys, Geogr. Helvetica, 74, 59–69, https://doi.org/10.5194/gh-74-59-2019, 2019.

Westermann, S., Ingeman-Nielsen, T., Scheer, J., Aalstad, K., Aga, J., Chaudhary, N., Etzelmüller, B., Filhol, S., Kääb, A., Renette, C., Schmidt, L. S., Schuler, T. V., Zweigel, R. B., Martin, L., Morard, S., Ben-Asher, M., Angelopoulos, M., Boike, J., Groenke, B., Miesner, F., Nitzbon, J., Overduin, P., Stuenzi, S. M., and Langer, M.: The CryoGrid community model (version 1.0) – a multi-physics toolbox for climate-driven simulations in the terrestrial cryosphere, Cryosphere, https://doi.org/10.5194/gmd-2022-127, 2022.

Winstral, A., Elder, K., and Davis, R. E.: Spatial Snow Modeling of Wind-Redistributed Snow Using Terrain-Based Parameters, J. Hydrometeorol., 3, 524–538, https://doi.org/10.1175/1525-7541(2002)003<0524:SSMOWR>2.0.CO;2, 2002.

Wirz, V., Schirmer, M., Gruber, S., and Lehning, M.: Spatio-temporal measurements and analysis of snow depth in a rock face, The Cryosphere, 5, 893–905, https://doi.org/10.5194/tc-5-893-2011, 2011.

Woo, M. and Heron, R.: Occurrence of Ice Layers at the Base of High Arctic Snowpacks, Arct. Alp. Res., 13, 225, https://doi.org/10.2307/1551198, 1981.

Woo, M., Heron, R., and Marsh, P.: Basal Ice in High Arctic Snowpacks, Arct. Alp. Res., 14, 251, https://doi.org/10.2307/1551157, 1982.

Zevenbergen, L. W. and Thorne, C. R.: Quantitative analysis of land surface topography, Earth Surf. Process. Landf., 12, 47–56, https://doi.org/10.1002/esp.3290120107, 1987.

Zhang, H., Aldana-Jague, E., Clapuyt, F., Wilken, F., Vanacker, V., and Van Oost, K.: Evaluating the potential of post-processing kinematic (PPK) georeferencing for UAV-based structure- from-motion (SfM) photogrammetry and surface change detection, Earth Surf. Dyn., 7, 807–827, https://doi.org/10.5194/esurf-7-807-2019, 2019.